doi:10.1093/brain/awx050

BRAIN
A JOURNAL OF NEUROLOGY

Selective impairment of hippocampus and posterior hub areas in Alzheimer's disease: an MEG-based multiplex network study

Meichen Yu,[1,*] Marjolein M. A. Engels,[2,*] Arjan Hillebrand,[1] Elisabeth C. W. van Straaten,[1,3] Alida A. Gouw,[1,2] Charlotte Teunissen,[4] Wiesje M. van der Flier,[2,5] Philip Scheltens[2] and Cornelis J. Stam[1]

*These authors contributed equally to this work.

Although frequency-specific network analyses have shown that functional brain networks are altered in patients with Alzheimer's disease, the relationships between these frequency-specific network alterations remain largely unknown. Multiplex network analysis is a novel network approach to study complex systems consisting of subsystems with different types of connectivity patterns. In this study, we used magnetoencephalography to integrate five frequency-band specific brain networks in a multiplex framework. Previous structural and functional brain network studies have consistently shown that hub brain areas are selectively disrupted in Alzheimer's disease. Accordingly, we hypothesized that hub regions in the multiplex brain networks are selectively targeted in patients with Alzheimer's disease in comparison to healthy control subjects. Eyes-closed resting-state magnetoencephalography recordings from 27 patients with Alzheimer's disease (60.6 ± 5.4 years, 12 females) and 26 controls (61.8 ± 5.5 years, 14 females) were projected onto atlas-based regions of interest using beamforming. Subsequently, source-space time series for both 78 cortical and 12 subcortical regions were reconstructed in five frequency bands (delta, theta, alpha 1, alpha 2 and beta band). Multiplex brain networks were constructed by integrating frequency-specific magnetoencephalography networks. Functional connections between all pairs of regions of interests were quantified using a phase-based coupling metric, the phase lag index. Several multiplex hub and heterogeneity metrics were computed to capture both overall importance of each brain area and heterogeneity of the connectivity patterns across frequency-specific layers. Different nodal centrality metrics showed consistently that several hub regions, particularly left hippocampus, posterior parts of the default mode network and occipital regions, were vulnerable in patients with Alzheimer's disease compared to control subjects. Of note, these detected vulnerable hubs in Alzheimer's disease were absent in each individual frequency-specific network, thus showing the value of integrating the networks. The connectivity patterns of these vulnerable hub regions in the patients were heterogeneously distributed across layers. Perturbed cognitive function and abnormal cerebrospinal fluid amyloid-β_{42} levels correlated positively with the vulnerability of the hub regions in patients with Alzheimer's disease. Our analysis therefore demonstrates that the magnetoencephalography-based multiplex brain networks contain important information that cannot be revealed by frequency-specific brain networks. Furthermore, this indicates that functional networks obtained in different frequency bands do not act as independent entities. Overall, our multiplex network study provides an effective framework to integrate the frequency-specific networks with different frequency patterns and reveal neuropathological mechanism of hub disruption in Alzheimer's disease.

1 Department of Clinical Neurophysiology and MEG Center, Neuroscience Campus Amsterdam, VU University Medical Center, Amsterdam, The Netherlands
2 Alzheimer Center and Department of Neurology, Neuroscience Campus Amsterdam, VU University Medical Center, Amsterdam, The Netherlands
3 Nutricia Advanced Medical Nutrition, Nutricia Research, Utrecht, The Netherlands

Received June 9, 2016. Revised December 22, 2016. Accepted January 14, 2017.

4 Neurochemistry lab and Biobank, Department of Clinical Chemistry, Neuroscience Campus Amsterdam, VU University Medical Center, Amsterdam, The Netherlands
5 Department of Epidemiology and Biostatistics, Neuroscience Campus Amsterdam, VU University Medical Center, Amsterdam, The Netherlands

Correspondence to: Meichen Yu,
Department of Clinical Neurophysiology and MEG Center,
VU University Medical Center,
De Boelelaan 1118,
1081 HV,
Amsterdam,
The Netherlands
E-mail: m.yu@vumc.nl

Keywords: Alzheimer's disease; hubs; heterogeneity; magnetoencephalography; multiplex network

Abbreviations: DMN = default mode network; MMSE = Mini-Mental State Examination; PLI = phase lag index

Introduction

Alzheimer's disease is a progressive neurodegenerative disorder. Clinically, Alzheimer's disease is characterized by early memory disturbances due to neurodegeneration in the entorhinal cortex and hippocampus, which gradually spreads to the temporal and parietal cortices and eventually entire cortex, as well as by disturbances in other cognitive domains (van der Flier and Scheltens, 2005; Querfurth and LaFerla, 2010; Ballard *et al.*, 2011; Scheltens *et al.*, 2016). Alzheimer's disease is defined neuropathologically by the accumulation of tau-containing extracellular neurofibrillary tangles and intracellular amyloid-β containing plaques (Blennow *et al.*, 2001; Schöll *et al.*, 2016). The pathology of these tangles and plaques causes cell loss and synaptic disruptions in specific cortical areas, which suggests that Alzheimer's disease can be described as a 'disconnection syndrome' (Buckner *et al.*, 2005; Arendt, 2009; Takahashi *et al.*, 2010; Dubois *et al.*, 2016). These microscopic alterations eventually can lead to macroscopic disruptions in, and between, distant brain areas (Scheltens *et al.*, 2016).

Electrophysiological and neuroimaging studies have revealed large-scale disruptions in structural and functional connections in Alzheimer's disease (Sperling, 2007; Buckner *et al.*, 2008; Greicius, 2008; Pievani *et al.*, 2011). However, pathology in Alzheimer's disease goes beyond disconnection and also affects network organization. Recent structural and functional network studies have reported that Alzheimer's disease is associated with a loss of small-world features (Stam *et al.*, 2007*a*, 2009; He *et al.*, 2008; de Haan *et al.*, 2009; Seeley *et al.*, 2009; Buldú *et al.*, 2011; Vecchio *et al.*, 2014), decreased nodal centrality in higher order association areas (Supekar *et al.*, 2008; Buckner *et al.*, 2009; de Haan *et al.*, 2012*a*; Canuet *et al.*, 2015; Dai *et al.*, 2015) and abnormal community structure (de Haan *et al.*, 2012*b*; Yu *et al.*, 2015, 2016; for reviews see: Tijms *et al.*, 2013; Stam, 2014; Fornito *et al.*, 2015). One of the most consistent findings is a selective vulnerability in cortical hub areas in Alzheimer's disease (Stam *et al.*, 2009; Lo *et al.*, 2010; de Haan *et al.*, 2012*c*; Crossley *et al.*, 2014; Dai *et al.*, 2015). Hubs are highly connected nodes, which occupy central positions in the overall organization of a network (van den Heuvel and Sporns, 2013). Albert and colleagues (2000) demonstrated that scale-free networks are robust to random attack (deleting randomly selected nodes), but vulnerable (lose structure and function) to targeted attack on hub nodes (deleting nodes in order of decreasing degree). Recent brain network studies also found that cortical hub areas are selectively vulnerable in many brain disorders, such as Alzheimer's disease (Buckner *et al.*, 2009; Stam *et al.*, 2009), schizophrenia (van den Heuvel *et al.*, 2010) and coma (Achard *et al.*, 2012). Of note, hubs in the posterior regions of the default mode network (DMN) consistently show high amyloid-β deposition in Alzheimer's disease (Buckner *et al.*, 2009), mild cognitive impairment (Drzezga *et al.*, 2011; Canuet *et al.*, 2015) and even older healthy subjects (Sperling *et al.*, 2009; Drzezga *et al.*, 2011).

Magnetoencephalography (MEG) directly measures oscillatory neuronal activity at the macroscopic scale with higher temporal resolution than functional MRI, and higher spatial resolution than routine electroencephalography (EEG) (Barkley, 2004; Baumgartner, 2004; Larson-Prior *et al.*, 2013; Jensen *et al.*, 2014). These properties make MEG a useful technique to map functional brain networks (Engel *et al.*, 2013; Lopes da Silva, 2013; van Diessen *et al.*, 2015). Conventionally, MEG connectivity and network analyses have been performed in different frequency bands separately, because different MEG rhythms are believed to reveal underlying biophysical properties of different local and global neural networks, and are also likely to be involved in different cognitive processes (Wang, 2010; Siegel *et al.*, 2012). Moreover, functional brain networks have been shown to be frequency-dependent (Bullmore and Sporns, 2009; Hillebrand *et al.*, 2012; Stam, 2014). For example, a recent MEG resting-state study in healthy subjects located hubs in medial temporal

lobe in the 4–6 Hz band, in lateral parietal areas in the 8–23 Hz band, and in sensorimotor areas for higher frequencies (32–45 Hz) (Hipp *et al.*, 2012). In Alzheimer's disease, MEG network studies have shown inconsistent results regarding hubs in different frequency bands. In earlier sensor-level MEG studies, we found that cortical hubs over the left temporal region are disrupted in the theta band in patients with Alzheimer's disease compared to healthy control subjects (de Haan *et al.*, 2012*a*), whereas patients with Alzheimer's disease showed higher functional connectivity over centro-parietal regions in the theta band and over occipito-parietal regions in the beta and gamma band (Stam *et al.*, 2006). There could be several reasons for these diverging results, one of them being that the frequency-specific functional networks should not be analysed in isolation, therefore requiring a unifying framework that integrates the frequency-specific networks and allows for the investigation of the topology across the different frequency bands.

Taking advantage of recent developments in the field of multiplex network theory (Kurant and Thiran, 2006; Buldyrev *et al.*, 2010; Kivelä *et al.*, 2014; Boccaletti *et al.*, 2014), the relationships between frequency-specific networks in MEG can be investigated (Brookes *et al.*, 2016; Tewarie *et al.*, 2016). In most real-world complex systems, a set of elementary entities interact with each other in multiple types of relationships. For instance, in a social network the network nodes, which are individuals, create friendships (network links) because they are e.g. teammates, colleagues, or because they are living together in a student house. Therefore, this social network can be considered as a multilayer network, where each type of relationship (teammate, colleague or housemate) between individuals consists of each network layer. The efficiency of information transfer between the individuals depends on the overall structure of the multilayer network, not just the structure of each specific layer. Information about a game might for example spread faster through the team because some team members also talk about it at dinner or at work, and not only during a training session. Therefore, to improve our understanding of complex systems consisting of multiple subsystems and layers of connectivity, it is important to take the 'multilayer' features into consideration. In a multilayer network, each layer consists of intraconnected sets of nodes, and nodes in different layers are interconnected by interlayer links. A multiplex network is the simplest case of a multilayer network, in which each layer shares the same set of nodes and the layers are interconnected only by the links between the same set of nodes across layers (Boccaletti *et al.*, 2014). Multiplex network theory has been applied in different real-world multiplex networks, such as air transportation systems (Cardillo *et al.*, 2013), social systems (Battiston *et al.*, 2014), interconnected hyperlink networks (De Domenico *et al.*, 2015) and massive multiplayer online games (Szell *et al.*, 2010). The topological properties of such systems are generally not present in single-layer subnetworks, but emerge due to the multilayer character of the systems (Cardillo *et al.*, 2013; Battiston *et al.*, 2014). Moreover, network percolation studies have demonstrated that the structural and dynamical properties of multiplex networks are radically different from those of single-layer networks (Havlin *et al.*, 2015). For instance, it has been demonstrated that single-layer scale-free networks are more robust under random attacks than targeted attacks on important hubs (Albert *et al.*, 2000). However, in the case of interdependent networks, hub nodes are particularly vulnerable when a random cascading failure occurs (Buldyrev *et al.*, 2010). Moreover, even when the hubs are protected, the multiplex scale-free networks are still vulnerable to random attacks (Huang *et al.*, 2011). Previous frequency-specific brain network studies have shown that hub regions in Alzheimer's disease are more vulnerable under targeted attack than random attack (Stam *et al.*, 2009; Crossley *et al.*, 2014), but it is unknown whether hub regions are also disrupted in multiplex networks in Alzheimer's disease. Therefore, it is important to study the hub properties in Alzheimer's disease in the framework of multiplex networks. In our study, the frequency-specific MEG-based networks can be naturally modelled as multiplex networks, where each frequency-specific network corresponds to a layer, and layers are interconnected by the links between the same set of brain regions across layers.

Here, we used eyes-closed resting-state MEG recordings from patients with Alzheimer's disease and control subjects to reconstruct the multiplex networks. We focused on the investigation of the overall hub properties and the participation of single hub areas (hub heterogeneity) to the structure of each layer (each frequency-specific MEG network), and in particular how these measures differed between the groups. We hypothesized that (i) the hub regions that play a central role in the multiplex brain networks in healthy controls are selectively different in patients with Alzheimer's disease; (ii) the heterogeneity of these vulnerable hub regions is different between patients with Alzheimer's disease and healthy control subjects; and (iii) hub vulnerability is associated with perturbed cognitive function and changes in protein biomarkers (CSF amyloid and tau) in patients with Alzheimer's disease.

Materials and methods

A schematic overview of the applied methods is provided in Fig. 1, which shows the processing steps, including beamforming for source reconstruction, filtering the source-space MEG data into five frequency bands, construction of the multiplex network and the graphic representation of the multiplex network measures.

Participants

The MEG recordings of the subjects have been analysed in our previous study (Engels *et al.*, 2016). The current study concentrates on a completely different research topic: multiplex

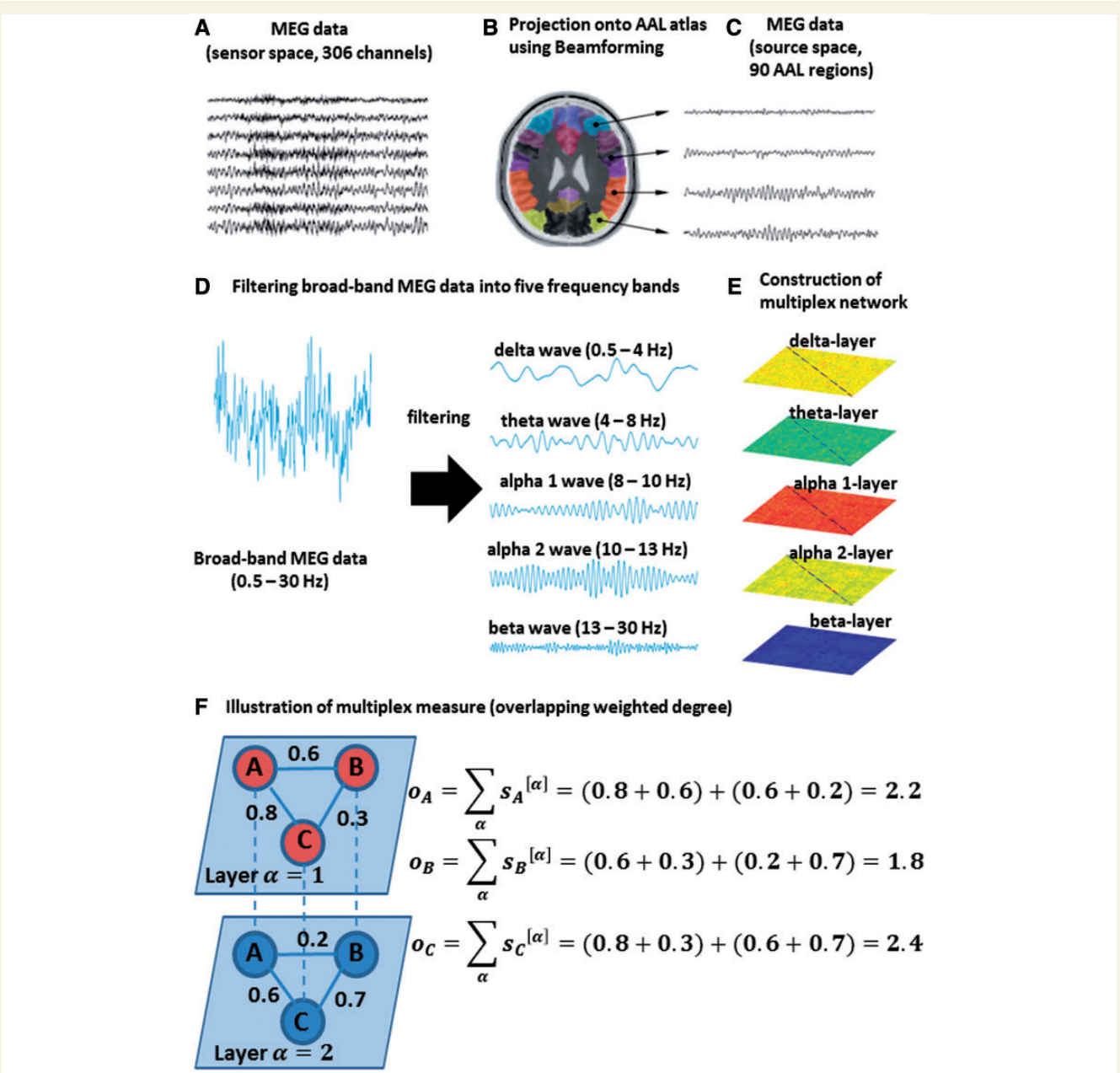

Figure 1 Schematic overview of the applied methods. Sensor space (306 channels) MEG data were recorded (**A**) and projected onto the AAL atlas using beamforming (**B**), resulting in 90 reconstructed time series of neuronal activation (**C**). These time series were then filtered into five frequency bands (delta: 0.5–4 Hz, theta: 4–8 Hz, alpha 1: 8–10 Hz, alpha 2: 10–13 Hz, beta: 13–30 Hz) (**D**). For each frequency band an adjacency matrix was constructed, containing the all-to-all connections between the filtered time-series. The connections were estimated using the PLI, which is a measure of functional connectivity that is relatively insensitive to the effects of field spread/signal leakage. The frequency-specific adjacency matrices formed the layers in a multiplex network (**E**). The topology of the multiplex network was estimated using various measures (overlapping weighted degree, overlapping weighted clustering coefficient, overlapping weighted local efficiency, overlapping weighted betweenness centrality and multiplex weighted participation coefficient), an example of which is given in (**F**) for the overlapping weighted degree. To simply illustrate the computation of overlapping weighted degree, an example for a two-layer multiplex network consisting of only two layers is shown in **F**. In our study, for all the multiplex network metrics we constructed multiplex networks consisting of five frequency-specific layers (as shown in **E**). **A–C** is modified, with permission, from Olde Dubbelink *et al.* (2014).

network analysis. Twenty-seven patients with probable Alzheimer's disease (age: 60.6 ± 5.4 years; 12 females) were included from the Amsterdam Dementia Cohort of the Alzheimer Center at the VU University Medical Center (van der Flier *et al.*, 2014). All patients fulfilled the National Institute of Aging-Alzheimer's Association (NIA-AA) criteria for probable Alzheimer's disease with a high likelihood of Alzheimer's disease pathophysiology, based on the

combination of a positive biomarker reflecting amyloid-beta (amyloid-β_{42}) deposition (in either CSF or by PET scanning) and/or a positive biomarker for neuronal injury (tau or phosphorylated tau in CSF). These biomarkers were assessed according to a standard diagnostic workup for dementia screening, which included an informant-based history of the patient (if available), physical, neurological and cognitive examinations, laboratory tests, structural brain imaging, and EEG. Diagnoses were made in a multidisciplinary consensus meeting. Patients gave written informed consent for use of their clinical data for research purposes (van der Flier *et al.*, 2014). Exclusion criteria for participation were: an active psychiatric or neurological disorder, Mini-Mental State Examination (MMSE) score below 18, or age above 70 years. In addition, we included 26 non-demented control subjects (age: 61.8 ± 5.5; 14 females) that had responded to an advertisement in a national newspaper. The matching of the controls and patients was done during the inclusion phase of the study. The patients were included first, and during the inclusion of the controls, we made sure that age and gender were not significantly different between the groups. After a telephone interview to exclude neurological or psychiatric disorders, subjects underwent neuropsychological testing, MRI of the brain and an MEG recording. All MEG recordings were obtained one to several hours before, or more than 1 week after the MRI scan to avoid interference due to, for example, magnetized dental elements. To avoid interference with the resting-state condition, neuropsychological testing of the control subjects was conducted after the MEG recording. In total, 31 subjects were invited of whom one was excluded as a meningioma was detected on the MRI; four volunteers were excluded due to poor performance during neuropsychological testing. The local Ethics Committee approved the study and all participants gave written informed consent before participation.

CSF biomarkers

CSF samples were obtained by lumbar puncture using a 25-gauge needle, and collected in 10 ml polypropylene tubes (Sarstedt) according to consensus protocols (Teunissen *et al.*, 2009). A small amount of the CSF was used for routine analysis including leucocyte count, erythrocyte count, glucose concentration, and total protein concentration. Within 2 h, the remaining CSF samples were centrifuged at 1800*g* for 10 min at 4°C, transferred to new polypropylene tubes, and stored at −20°C until routine biomarker analysis (within 2 months). Amyloid-β_{42}, total tau, and p-tau were measured with commercially available ELISAs [INNOTEST® amyloid-β (1-42), INNOTEST® hTAU-Ag and INNOTEST® Phosphotau$_{(181P)}$, respectively; Fujirebio] on a routine basis as described before (Mulder *et al.*, 2010). Intra-assay coefficients of variation [CVs; mean ± standard deviation (SD)] were 2.0 ± 0.5% for amyloid-β_{42}, 3.2 ± 1.3% for tau, and 2.9 ± 0.8% for p-tau, as calculated from averaging CVs of duplicates from five runs randomly selected over 2 years. Inter-assay CVs (mean) were 9.5% for amyloid-β_{42}, 11.4% for tau, and 12% for p-tau, as analysed in 88–96 samples of a high and low pool (one normal and one Alzheimer's disease profile) over nine different kit lots used during the whole study period.

MEG recording

Several weeks after diagnostic work-up, MEG recordings were made in a magnetically shielded room (VacuumSchmelze) using a 306-channel whole-head system (Elekta Neuromag Oy). For each subject, the recording protocol consisted of at least 5 min (range 300–394 s) of eyes-closed resting-state condition followed by 2 min eyes-open, and again at least 5 min eyes-closed (range 300–394 s). In this protocol, to ensure that the subjects stayed awake during recording, we asked them to open their eyes for 2 min after 5 min. To avoid potential confounders due to eye blinks during the eyes-open condition, and because EEG parameters during the eyes-closed condition are more stable over sessions (Corsi-Cabrera *et al.*, 2007), we only analysed the second 5-min eyes-closed data segment (van Diessen *et al.*, 2015). The recordings were sampled at 1250 Hz, with an online anti-aliasing filter (410 Hz) and high-pass filter (0.1 Hz). Offline, a spatial filter, the temporal extension of Signal Space Separation (tSSS) (Taulu and Simola, 2006; Taulu and Hari, 2009), as implemented in MaxFilter software (Elekta Neuromag Oy, version 2.2.10), was applied with a sliding window of 10 s. Channels containing excessive artefacts were discarded after visual inspection of the data by one of the authors (M.E.) before estimation of the SSS coefficients. The number of excluded channels varied between one and 12. After fine-tuning for acquisition conditions at our site, the tSSS filter was used to remove noise signals that SSS failed to discard, typically from noise sources near the head, using a subspace correlation limit of 0.9 (Medvedosky *et al.*, 2009; Hillebrand *et al.*, 2013; Tewarie *et al.*, 2014). Typical artefacts were due to (eye) movements, swallowing, dental prosthetics, or drowsiness, although the subjects were instructed to stay awake and reduce eye movements during the MEG recording. The head position relative to the MEG sensors was recorded continuously using the signals from four head localization coils. The head localization coil positions were digitized, as well as the outline of the participant's scalp (~500 points), using a 3D digitizer (Fastrak). This scalp surface was used for co-registration with the patient's MRI scan.

Structural scans

Structural MRI scans were made of all participants except for one patient. This patient had an MRI of insufficient quality and therefore we used a CT scan for structural information of the scalp outline. The outline of the scalp on the structural scans was extracted using segmentation (SEGLAB; Elekta Neuromag Oy, version 2.0.15). Co-registration of the MEG data with the structural scans was achieved using surface matching, resulting in an estimated co-registration accuracy of ~4 mm (Whalen *et al.*, 2008). Visual inspection of the co-registration between the MEG and the MRI/CT scalp surfaces was performed for all patients. The sphere that best fitted the scalp surface was used as a volume conductor model for the beamformer analysis (see below).

Source reconstruction using beamforming

To obtain source-localized activity, we applied an atlas-based beamforming approach (Hillebrand *et al.*, 2012). Sensor

signals were projected to an anatomical framework such that source-reconstructed neuronal activity for 78 cortical and 12 subcortical regions of interest, identified by means of automated anatomical labeling (AAL) (Tzourio-Mazoyer *et al.*, 2002), were obtained. Each region of interest contains many voxels and due to different region of interest shapes, the number of voxels is different for every region of interest. To obtain a single time series for a region of interest, we selected the centroid voxel as representative for a specific region of interest (Hillebrand *et al.*, 2016). For each centroid, broad band (0.5–48 Hz) beamformer weights were computed using the data covariance matrix and the forward solution (lead field) of a dipolar source at the voxel location (van Veen *et al.*, 1997; Robinson and Vrba, 1999; Hillebrand *et al.*, 2005). A time window of, on average, 277 s (range 105–435 s) was used to compute the data covariance matrix. Singular value truncation was used when inverting the data covariance matrix to deal with the rank deficiency of the data after SSS (~70 components). Then the time series for each centroid, i.e. a virtual electrode, was reconstructed by projecting the broad band data through the normalized beamformer weights (van Veen *et al.*, 1997; Robinson and Vrba, 1999; Hillebrand *et al.*, 2005; Cheyne *et al.*, 2007). For each subject, care was taken to select 20 artefact-free source-projected epochs of 4096 samples (3.2768 s) by one of the authors (M.E.). A second researcher independently evaluated the selected epochs (I.N.). Epochs without consensus were replaced by new epochs. Epochs were converted to ASCII-format and imported into an in-house (C.S.) developed software package (BrainWave version 0.9.125.2.7; http://home.kpn.nl/stam7883/brainwave.html). The MEG data were digitally filtered off-line with a band pass filter of 0.5–30 Hz using a discrete Fast Fourier transform, following which the relative power, averaged over the selected epochs, was estimated for the following frequency bands: delta (0.5–4 Hz), theta (4–8 Hz), lower alpha (8–10 Hz), upper alpha (10–13 Hz), beta (13–30 Hz). All real and imaginary components of the Fourier transform outside the pass band were set to 0, following which an inverse Fourier transform was used to obtain the filtered time series for the different frequency bands.

Functional connectivity analysis and multiplex network construction

The assessment of MEG functional connectivity could be influenced by primary and secondary leakage (Schoffelen and Gross, 2009; Brookes *et al.*, 2011*a*; Palva and Palva, 2012). In MEG a single source produces a signal at multiple recording sites, known as field spread, or (primary) signal leakage in source space, which can give rise to spurious estimates of functional connectivity (Schoffelen and Gross, 2009). Moreover, this leakage may also result in spurious estimates of connectivity ('inherited connectivity' or 'secondary leakage') between areas surrounding two genuinely connected brain regions (Palva and Palva, 2012).

As a measure of functional connectivity between all pair-wise combinations of regions of interest, the phase lag index (PLI) was used to compute the asymmetry of the distribution of phase differences [$\Delta\,\varphi(t_k)$, t_k corresponds to time samples $1 \cdots N_k$] between any two time series (Stam *et al.*, 2007*b*). The instantaneous phase difference between pair-wise signals can be determined using the analytical signal as obtained from the Hilbert transform (Rosenblum *et al.*, 1996). Both modelling (Stam *et al.*, 2007*b*; Porz *et al.*, 2014) and experimental (Hillebrand *et al.*, 2012) studies have shown that the PLI is relatively insensitive to the effects of field spread or (primary) signal leakage (for secondary leakage, see 'Statistical analysis' section), and is computed as:

$$\mathrm{PLI} = |\langle \mathrm{sign}[\sin(\Delta\,\varphi(t_k))]\rangle| \quad (1)$$

Here, $< >$ denotes the mean value, sign stands for the signum function and $||$ indicates the absolute value. The PLI values range between 0 [no consistent coupling, or coupling with zero lag (modulus π)] and 1 [perfect (non-zero delay) phase locking].

For each epoch, and for each of the five frequency bands, a square 90×90 weighted adjacency matrix was constructed from the PLI value between all pair-wise combinations of the 90 regions of interest.

The multiplex networks were reconstructed by integrating the five frequency-specific PLI-weighted networks, where each layer shared the same set of nodes (90 AAL regions of interest), but the links in each layer were formed by the PLI-weighted functional connections within each frequency band. The layers were interconnected only by the links between the same set of nodes across layers, so in this study the cross-frequency couplings between different brain regions were not considered (Jensen and Colgin, 2007; Brookes *et al.*, 2016; Tewarie *et al.*, 2016).

The MEG multiplex network for each epoch consisted of N ($N = 90$) nodes and M ($M = 5$) weighted layers α ($\alpha = 1, \ldots, M$). For each layer α, the corresponding adjacency matrix is $A^{[\alpha]} = \{\omega_{ij}^{[\alpha]}\}$, where $\omega_{ij}^{[\alpha]} = \mathrm{PLI}$ (see Equation 1) if node i and node j are connected through a PLI-weighted link on layer α. The five-layer multiplex network is specified by the vector of the adjacency matrices $A = \{A^{[1]}, \ldots, A^{[M]}\}$ (Battiston *et al.*, 2014).

Multiplex network topology

Multiplex centrality metrics

We first investigated the hub properties of the multiplex networks. Hub properties can be characterized using different centrality metrics, capturing different aspects of centrality. We considered four different centrality metrics: weighted degree (or node strength), weighted clustering coefficient, weighted local efficiency, weighted betweenness centrality. The weighted centrality metrics were computed using the Brain Connectivity Toolbox (BCT) (Rubinov and Sporns, 2010).

We generalized the considered centrality metrics in the framework of multiplex networks. The weighted degree of a node i on layer α is $s_i^{[\alpha]} = \sum_j \omega_{ij}^{[\alpha]}$. The weighted degree of node i in a multiplex network can also be represented as a vector,

$$s_i = \left\{s_i^{[1]}, \ldots, s_i^{[M]}\right\}, i = 1, \ldots, N. \quad (2)$$

For node i, the overlapping weighted degree is

$$o_i = \sum_{\alpha} s_i^{[\alpha]}. \quad (3)$$

The detailed description of weighted clustering coefficient (c_i), weighted local efficiency (e_i), weighted betweenness centrality (b_i) and corresponding overlapping formations can be found in the Supplementary material. Note that all the multiplex centrality metrics (overlapping weighted degree, overlapping weighted clustering coefficient, overlapping weighted local efficiency, overlapping weighted betweenness centrality), were first computed for each node in each layer separately, and then summed up across five frequency-specific (delta, theta, alpha 1, alpha 2 and beta) layers. The multiplex centrality metrics were computed for each node i (AAL region) for each epoch and for each subject. The link weights in different layers may have different magnitudes, which may cause biases for the estimation of multiplex centrality metrics and for the comparison between multiplex networks (Stam *et al.*, 2014). To minimize the potential biases caused by the different magnitudes of link weights, the link weights within each layer were first ranked in increasing order, and then assigned natural numbers starting from 1. All the multiplex centrality metrics were re-computed based on the ranked link weights.

Hub disruption of multiplex networks

To compare the nodal centrality (hub) properties between the Alzheimer's disease and healthy control groups, we computed the hub disruption index (Achard, *et al.*, 2012). For a given nodal centrality measure, for instance the overlapping weighted degree, we first computed the mean overlapping weighted degree, i.e. averaged over epochs and subjects, of multiplex networks in the healthy control group. Next, we subtracted the mean overlapping weighted degree of the healthy group $o_{\langle control_i \rangle}$ from the overlapping weighted degree of the corresponding node i in one epoch for one patient with Alzheimer's disease $o_{Alzheimer's\ disease_i}$, which was then plotted against $o_{\langle control_i \rangle}$. This was repeated for each node. The hub disruption index (k) for the epoch of the patient with Alzheimer's disease is the linear regression coefficient (least-squares first-order polynomial fit) of the regression line fitted to the resulting scatter plot (Supplementary Fig. 3). The same procedure was also performed for each epoch of each subject in the healthy control group. The hub disruption index was therefore estimated for all of the epochs of the subjects in both groups. The significance of a between-group difference in the hub disruption index was estimated using permutation testing (for details, see the 'Statistical analysis' section). We assumed that the nodal centrality for a healthy subject is similar to the average of the healthy controls, and that in Alzheimer's disease the largest hubs are most disrupted ($k < 0$). In this case, the regression line for the controls would be horizontal ($k \sim 0$), whereas the regression line for the patients with Alzheimer's disease would have a negative slope (Supplementary Fig. 3).

In this study, the values of the multiplex centrality metrics and corresponding hub disruption indices were used to quantify the vulnerability of hub regions in patients with Alzheimer's disease.

Heterogeneity of multiplex networks

For a multiplex network, two nodes i and j may have, for example, exactly the same overlapping weighted degree ($o_i = o_j$), yet have different weighted degree distributions across different layers, and therefore play different roles in the multiplex network. To characterize the heterogeneity of the connectivity patterns in the five-layer MEG multiplex networks, we first performed conventional statistical analyses (Fig. 5), such as the computation of the mean and standard deviations of the weighted degrees for each region across five frequency-specific layers, and the pair-wise correlations of the five weighted degree sequences. Then, we will demonstrate that the multiplex participation coefficient (Battiston *et al.*, 2014), another multiplex network measure, can also be used to reveal this heterogeneity across layers in the framework of a multiplex network (Fig. 6).

The definition of the multiplex participation coefficient is based on the definition of the participation coefficient in a single-layer network, which quantifies the participation of a node in different communities (Guimerà and Nunes Amaral, 2005). In this adaptation to the MEG multiplex networks, the multiplex participation coefficient quantifies the participation of each brain region in the five different frequency-specific layers. For a node i, the multiplex participation coefficient is defined as

$$P_i = \frac{M}{M-1}\left[1 - \sum_{\alpha=1}^{M}\left(\frac{s_i^{[\alpha]}}{o_i}\right)^2\right] \quad (4)$$

The P_i ranges between 0 (the weighted degree of node i concentrates in one layer only) and 1 (node i has the same weighted degree in each of the M layers). In general, the larger the value of P_i, the more homogenous the weighted degree distribution of node i across the M layers is. Importantly, if most nodes in the multiplex network have relatively high P_i value, that is, most nodes are homogenously distributed across layers, then the multiplexity of the constructed network is more prominent. The overall participation coefficient of the whole multiplex network is defined as the mean value of P_i over all nodes, $P = \frac{1}{N}\sum_i P_i$. Here, we defined nodes with relatively high multiplex participation coefficient as connectors between different layers of the multiplex networks; inversely, nodes with relatively low multiplex participation coefficient were defined as peripheral nodes that mainly interact with the nodes within their own layers.

In this study, we concentrated on the degree-based multiplex participation coefficient. To classify the role of each node in the five-layer multiplex networks, we considered the overlapping weighted degree o_i and multiplex participation coefficient P_i at the same time, that is, the Spearman's rank correlation between the overlapping weighted degree and multiplex participation coefficient was computed. Positive correlations would indicate that hub nodes would also tend to act as connectors across frequency bands, and that non-hub nodes would tend to be peripheral nodes. Group-level comparisons were performed by permutation testing (for details, see the 'Statistical analysis' section). To directly compare the nodal heterogeneity between patients with Alzheimer's disease and controls, the hub disruption index based on the multiplex participation coefficient was also computed.

Functional connectivity analysis and multiplex network analyses were performed with BrainWave software (BrainWave version 0.9.125.2.7; http://home.kpn.nl/stam7883/brainwave.html) and MATLAB (MathWorks, Natick, Massachusetts,

U.S.A.; Version R2015a), respectively. The nodal centrality metrics were visualized with BrainNet Viewer (version 1.5, Xia *et al.*, 2013, http://www.nitrc.org/projects/bnv/).

Statistical analysis

Statistical analyses of group characteristics were performed with IBM SPSS Statistics 21. Differences between groups in age, MMSE and education were tested using unpaired Student's *t*-tests, while gender differences between groups were tested using a chi-square test.

Permutation tests were used to compare multiplex network metrics between patients with Alzheimer's disease and control subjects. Both group- and subject-level comparisons were performed in the permutation tests to reduce potential biases that either approach may have (see Supplementary material for details). The *P*-values for all pair-wise comparisons were corrected by false discovery rate (FDR) (Benjamini and Hochberg, 1995). As exploratory *post hoc* analyses, Spearman's correlations between the nodal centrality metrics (overlapping weighted degree o_i, overlapping weighted clustering coefficient c_i, overlapping weighted local efficiency e_i and overlapping weighted betweenness centrality b_i) and MMSE scores for regions which showed significantly different nodal centrality values between the two groups: left superior occipital gyrus (SOG.L) (o_i, c_i, e_i), left middle occipital gyrus (MOG.L) (o_i, c_i, e_i), left inferior occipital gyrus (IOG.L) (o_i, c_i, e_i), right superior parietal gyrus (SPG.R) (o_i, c_i, e_i), left superior parietal gyrus (SPG.L) (e_i), right inferior parietal, but supramarginal and angular gyri (IPL.R) (o_i,c_i,e_i), right precuneus (PCUN.R) (o_i, c_i, e_i), right cuneaus (CUN.R) (c_i, e_i), left hippocampus (HIP.L) (o_i, c_i, e_i), right superior frontal gyrus, dorsolateral (SFGdor.R) (b_i); in total, correlations for 25 regions or variables (25 comparisons) were computed. Moreover, the correlations between the four hub disruption indices and MMSE, and three CSF biomarkers (amyloid-β_{42}, p-tau and tau) were computed ($4 \times 4 = 16$ comparisons). The correlation analyses were performed using IBM SPSS Statistics 21. For the correlation analyses, the correction for multiple testing was not performed. A significance level of $\alpha < 0.05$ was used for all the statistical analyses.

In our study, we tested if the observed group differences of multiplex network measures could be explained by differences in secondary leakage (Palva and Palva, 2012). To this end, we compared (permutation test with FDR correction) the mean absolute correlations between beamformer weights for each region of interest between the two groups (Brookes *et al.*, 2011*a*; Hillebrand *et al.*, 2012) (Supplementary material).

Results

Demographics

Subject characteristics, cognitive scores and CSF biomarkers, are presented in Table 1. Age and gender did not differ between the two groups. The mean MMSE score was lower in patients with Alzheimer's disease compared to the healthy controls. CSF data were only available for patients with Alzheimer's disease, but were all in the range of a typical Alzheimer's disease profile and are presented as the median and interquartile range.

Table 1 Subject characteristics, cognitive scores and CSF biomarkers

	Alzheimer's disease	Healthy control
n	27	26
Gender (F/M)	12/15	14/12
Mean age (SD)	60.6 (5.4)	61.8 (5.5)
Mean MMSE score (SD)	23.4 (2.6)*	28.9 (1.0)
CSF amyloid-β_{42} (range, pg/ml)	533 (435–599)	n.a.
CSF tau (range, pg/ml)	663 (399–984)	n.a.
CSF p-tau (range, pg/ml)	79 (53–104)	n.a.

F = females; M = males; *n* = number of subjects; n.a. = not available; p-tau = phosphorylated at threonine 181; SD = standard deviation.
Independent Student *t*-tests or chi-square tests were used when applicable. Age and MMSE score are presented as mean and standard deviation; CSF biomarkers are presented as median (interquartile range). CSF biomarkers are only available for 24 patients with Alzheimer's disease. *$P < 0.01$.

Multiplex centrality metrics

The mean overlapping weighted degree values are presented in Fig. 2A and B for Alzheimer's disease and control subjects, respectively. The controls showed an anterior-to-posterior increase for all the given nodal centrality metrics (Fig. 2B and Supplementary Fig. 1). Compared with controls, the overlapping weighted degree was significantly lower in Alzheimer's disease in the left hippocampus, right precuneus, two right parietal regions (superior parietal cortex and inferior parietal cortex), and three left occipital regions (superior, middle, and inferior occipital cortex) (Fig. 2A and C, and Supplementary Fig. 1). Most of these regions had relatively high overlapping weighted degree in the control subjects, in particular the right precuneus (highest) and right inferior parietal cortex (third highest), which consists of posterior components of default mode network (Fig. 2B). The selectively disrupted hub brain areas in patients with Alzheimer's disease were consistently found across regional centrality measures (Supplementary Fig. 1). The results were also consistent by using the rank number of the link weights within each layer instead of the original PLI values (Supplementary Fig. 2). The above significant group differences obtained for the multiplex brain networks could not be revealed by individually considering each of the five frequency-specific networks. For the delta and alpha 2-band networks, the weighted degrees between the two groups were different in only two parietal and one temporal non-hub brain regions, respectively (Fig. 3); no significant differences were found in the other frequency bands.

In summary, multiplex hub areas, including the medial temporal lobe, posterior DMN and occipital cortex were selectively disrupted in patients with Alzheimer's disease.

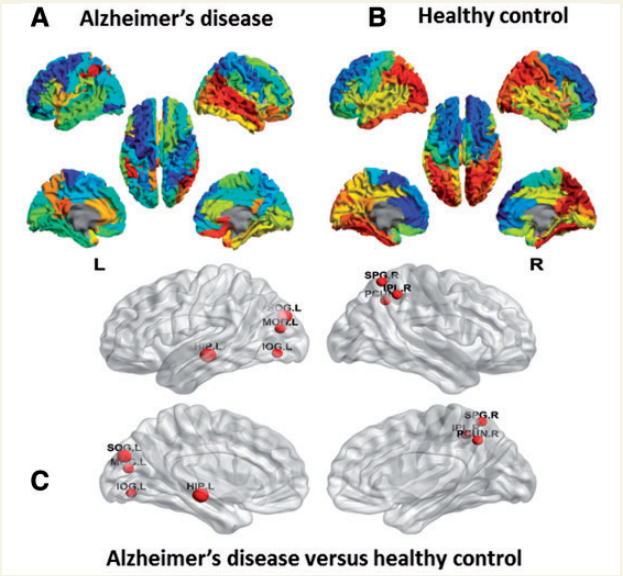

Figure 2 Vulnerability of hub regions in patients with Alzheimer's disease. The mean overlapping weighted degree for each region of interest displayed as a colour-coded map on the parcellated template brain in patients with Alzheimer's disease (**A**) and healthy controls (**B**). (**C**) Cortical surface representation of the regions that demonstrated significant between-group difference in overlapping weighted degree; permutation tests with FDR correction. See Supplementary Fig. 1 for corresponding results for other nodal centrality metrics (overlapping weighted local efficiency, overlapping weighted clustering coefficient, overlapping weighted betweenness centrality). PCUN.R = right precuneus; HIP.L = left hippocampus; IPL.R = right inferior parietal, but supramarginal and angular gyri; SPG.R = right superior parietal gyrus; MOG.L = left middle occipital gyrus; SOG.L = left superior occipital gyrus; IOG.L = left inferior occipital gyrus. A full list of labels (abbreviations) used for the different brain areas can be found in Supplementary Table 2.

Hub disruption of multiplex networks

The abnormal patterns of nodal centrality in Alzheimer's disease were confirmed by computing the hub disruption index (k) for each metric. For the overlapping weighted degree, patients with Alzheimer's disease showed a negative hub disruption index ($k = -0.8079$) compared with the controls ($k = 0.0605$; $P = 0.00014$) (Supplementary Table 1); in other words, the regions with relatively high overlapping weighted degrees (for instance, the right precuneus and right inferior parietal cortex) in controls showed the greatest reduction in patients with Alzheimer's disease, whereas the regions with relatively low overlapping weighted degrees (e.g. prefrontal regions) in controls showed the greatest enhancement in patients with Alzheimer's disease (Fig. 4). Moreover, the results were also consistent for the other nodal hub metrics (Supplementary Table 1). These results demonstrate that multiplex brain networks in Alzheimer's disease were not only disrupted selectively in specific brain areas, but also at a whole-brain level. Moreover, the abnormal topologies of the multiplex networks in patients with Alzheimer's disease results from the shift of centrality status from the medial temporal lobe (hippocampus) and posterior regions (parietal and occipital areas) to prefrontal regions.

Heterogeneity of multiplex networks

As can be seen in Fig. 5A, the weighted degrees were highest in the alpha 1-band single-layer network, but lowest in the beta-band single-layer network in both Alzheimer's disease and control groups. For the majority of brain regions, the standard deviations of the weighted degrees across the five layers were lower for patients with Alzheimer's disease than for the controls, indicating that for most brain regions the weighted degrees were less heterogeneously distributed across the frequency bands in patients with Alzheimer's disease than in control subjects (Fig. 5B). In Fig. 5C, we ranked the weighted degrees within each frequency-specific network for the two groups, respectively. By visual inspection, in both groups the five weighted degree sequences appeared weakly (anti)correlated, with the regions which are hubs in one layer often having low weighted degree in other layers. To quantify the correlations of the weighted degree sequences, we computed the Spearman's rank correlations between pairs of layers in both groups (Fig. 5D). We found that, in both groups, the weighted degrees sequences of pairs of layers were only weakly correlated: in patients with Alzheimer's disease, the delta and alpha 2 layers were anti-correlated; in controls, the theta and alpha 1 layers were correlated, which was even weaker in patients with Alzheimer's disease; the alpha 1 and alpha 2 layers were anti-correlated in controls, but were correlated in patients with Alzheimer's disease. These results suggest the existence of nodal heterogeneity of weighted degree distributions across layers in MEG-based multiplex networks, indicating that brain regions play different roles in different frequency-specific networks.

To quantify and compare the heterogeneity of the multiplex brain networks in Alzheimer's disease patients and control subjects further, we considered the overlapping weighted degree and multiplex participation coefficient at the same time by mapping the 2D P_i-o_i plane for both groups (Fig. 6A). In patients with Alzheimer's disease, the P_i was negatively correlated with o_i (Spearman's $r = -0.2921$, $P = 0.0054$), indicating that the weighted degrees of hub regions in patients with Alzheimer's disease are less homogeneously distributed across layers than those of non-hub regions. In contrast, for the control subjects the weighted degree distributions of the hub regions were more homogeneously distributed across layers than those of non-hub regions (Spearman's $r = 0.1362$, $P = 0.2001$). These correlation coefficients differed ($P = 0.0013$), indicating that the hub regions of the multiplex brain networks in patients with Alzheimer's disease were less heterogeneously distributed across layers than those in controls.

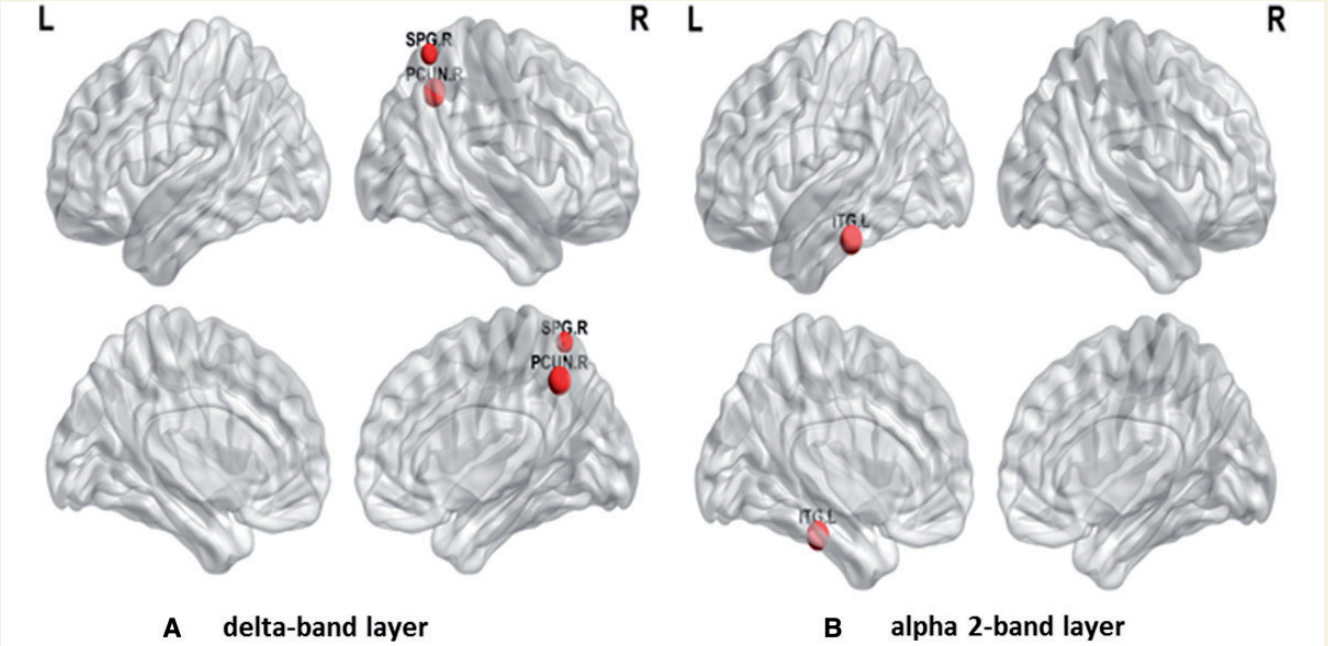

Figure 3 Vulnerability of hub regions in frequency-specific brain networks in patients with Alzheimer's disease. Cortical surface representation of the regions that showed significant between-group difference in weighted degree between Alzheimer's disease and healthy controls for the delta-band layer [right precuneus (PCUN.R) and superior parietal gyrus (SPG.R)] (**A**) and alpha 2-band layer (inferior temporal gyrus, ITG.L) (**B**); permutation tests with FDR correction.

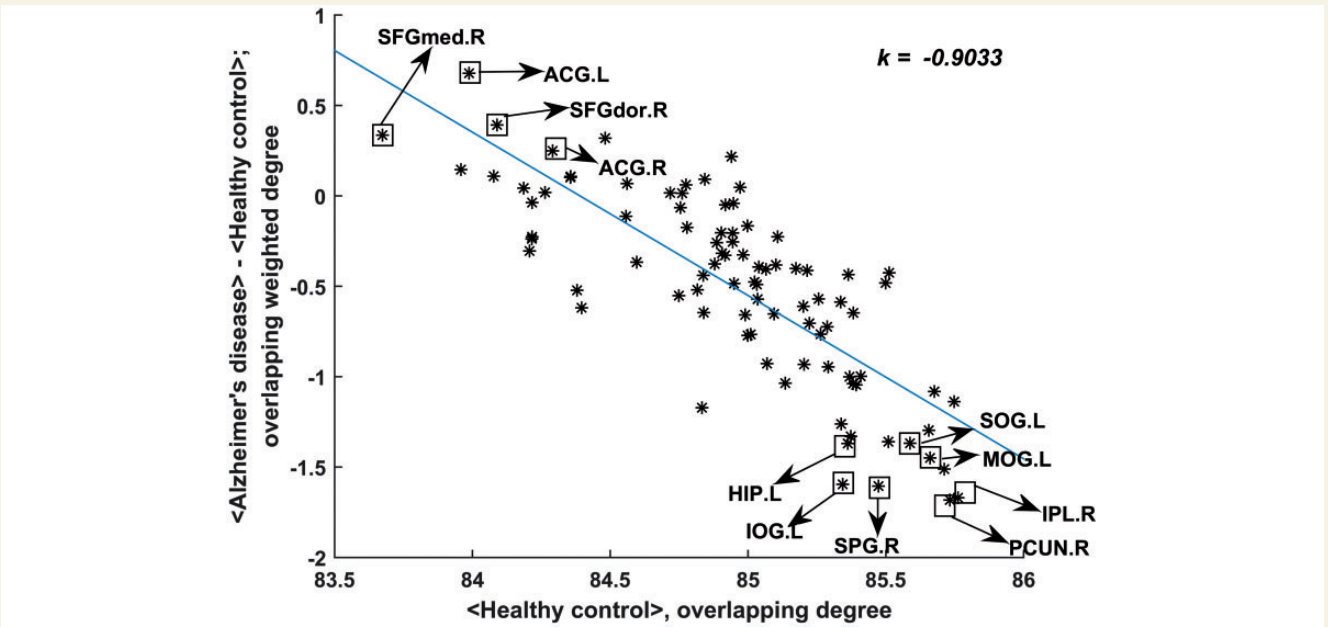

Figure 4 Hub disruption of functional networks in patients with Alzheimer's disease. The difference between groups in mean overlapping weighted degree of each node Alzheimer's disease – healthy control is plotted against the mean overlapping weighted degree of each node in the healthy control healthycontrol group. The hub brain areas have a high mean overlapping weighted degree in the healthy group and an abnormal reduction of overlapping weighted degree in the Alzheimer's disease group, e.g. right precuneus (PCUN.R), left hippocampus (HIP.L), right inferior parietal, but supramarginal and angular gyri (IPL.R) and right superior parietal gyrus (SPG.R), whereas regions that are non-hubs have a low local efficiency in controls and an abnormal increase of overlapping weighted degree in Alzheimer's disease, e.g. prefrontal regions: right superior frontal gyrus, medial (SFGmed.R), right superior frontal gyrus, dorsolateral (SFGdor.R), left anterior cingulate and paracingulate gyri (ACG.L) and right anterior cingulate and paracingulate gyri (ACG.R). These results indicate that the hub properties in patients with Alzheimer's disease were disrupted in parietal and hippocampus regions, but enhanced in the prefrontal regions. Note that Fig. 4 aims to show how hub disruption index is able to reveal the disruption of hub areas in patients with Alzheimer's disease. The boxes, arrows and corresponding text were used to label the corresponding regions. In this study, we performed the permutation tests to compare the hub disruption indices between patients with Alzheimer's disease and controls (for details, see the 'Statistical analysis' section and Supplementary Fig. 3).

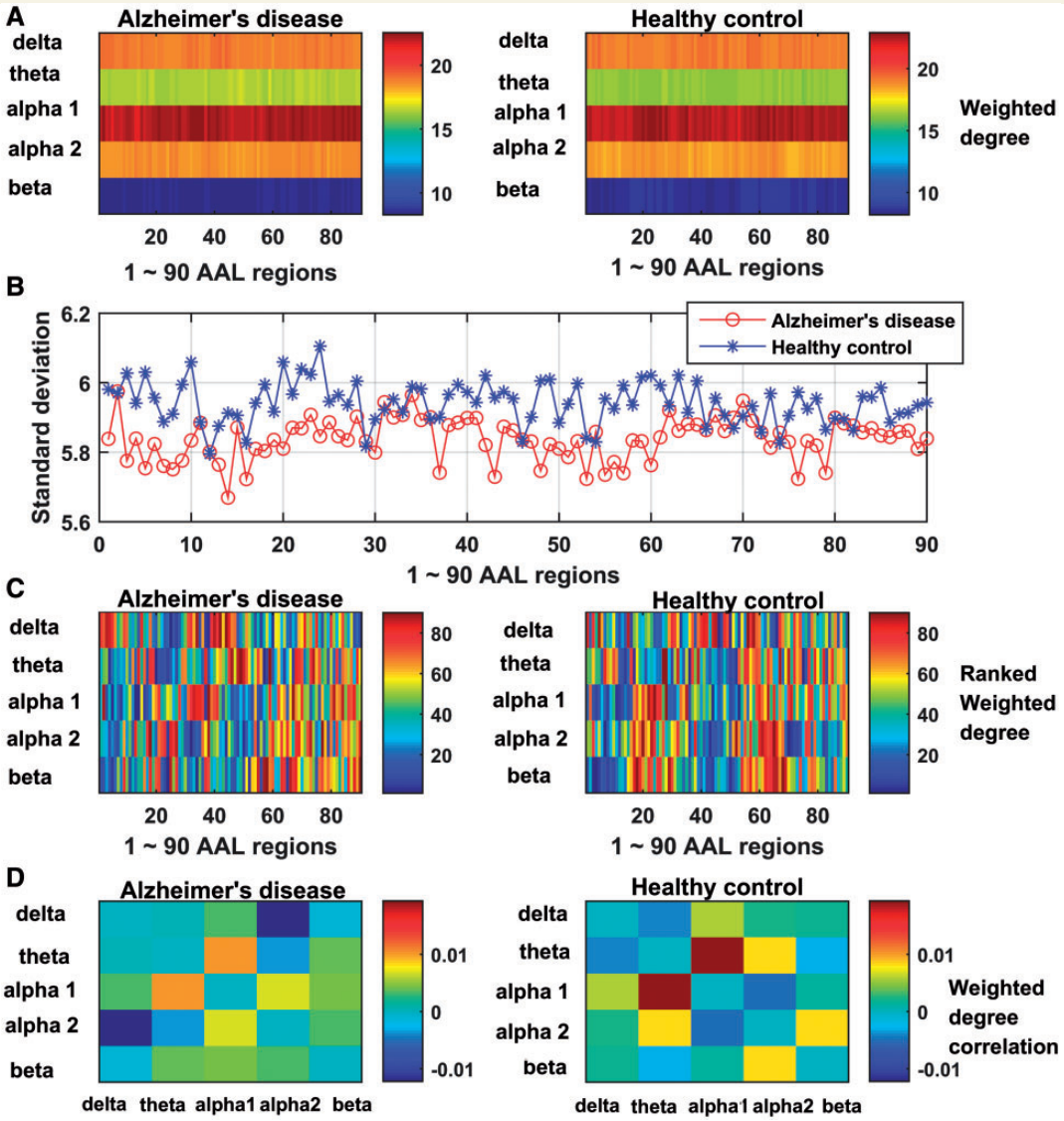

Figure 5 Heterogeneity of multiplex networks in patients with Alzheimer's disease and healthy controls. Mean (**A**) and standard deviation (**B**) of the weighted degrees for each region for five single-layer frequency-specific networks in patients with Alzheimer's disease and healthy controls. (**C**) Ranked weighted degrees of each region for five single-layer frequency-specific networks in patients with Alzheimer's disease and healthy controls. (**D**) Weighted degree correlations between pairs of layers in patients with Alzheimer's disease and healthy controls. Note that to emphasize the correlations between different layers, we set all the self-correlations equal to 0. The correspondent AAL labels of the Arabic numerals (1∼90 AAL regions) in the *x*-axis of **A–C** can be found in Supplementary Table 2.

The hub regions in patients with Alzheimer's disease included the vulnerable regions detected by the nodal centrality metrics (here, overlapping weighted degree), which revealed different nodal heterogeneity in Alzheimer's disease and healthy control groups (*cf.* Fig. 2C and labelled regions of interest in Fig. 6A). Notably, some vulnerable hub regions played different roles in Alzheimer's disease compared to controls: the vulnerable posterior DMN regions, including the right precuneus and inferior parietal regions, were peripheral hub regions in controls, but were non-hub connectors in patients with Alzheimer's disease. However, other vulnerable hub regions showed similar nodal heterogeneity in the two groups: the left hippocampus and superior parietal regions were connectors in both groups; the three occipital regions (superior, mid and inferior occipital regions) were peripheral nodes in both groups. These results indicate that although the hub regions in controls not only consistently lost their nodal efficiency in patients with Alzheimer's disease, but also showed differences in nodal heterogeneity across layers in the two groups. The difference in nodal heterogeneity between the two groups was further confirmed by performing the subject-level hub disruption analysis: the multiplex participation coefficient in patients with Alzheimer's disease showed a more negative hub disruption index ($k = -0.9089$) in comparison with that ($k = 0.0565$) of controls ($P = 0.0002$) (Fig. 6B and Supplementary Table 2). In summary, the multiplex participation coefficient quantified the relationships

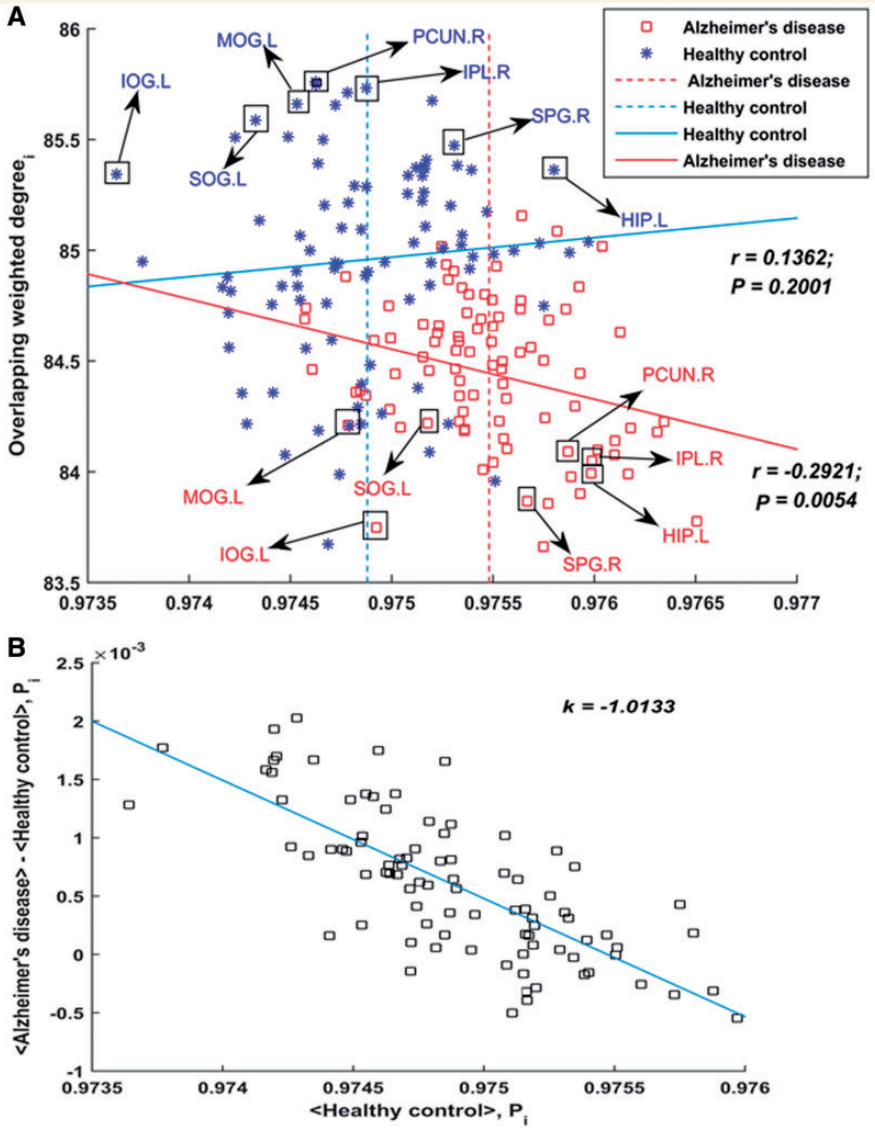

Figure 6 The heterogeneity of the multiplex networks in patients with Alzheimer's disease and healthy controls. (**A**) 2D P_i-o_i parameter space of the mean multiplex network in patients with Alzheimer's disease and healthy controls. (**B**) Hub disruption of the multiplex participation coefficient (k) in patients with Alzheimer's disease; permutation test with FDR correction. Note that only the significantly vulnerable hub regions identified in Fig. 2C were labelled. Note that in **A** the vertical dashed lines indicate the mean P_i values; the solid lines indicate the regression lines fitted to the scatter plots; the red and blue colours indicate patients with Alzheimer's disease and healthy controls, respectively. PCUN.R = right precuneus; HIP.L = left hippocampus; IPL.R = right inferior parietal, but supramarginal and angular gyri; SPG.R = right superior parietal gyrus; MOG.L = left middle occipital gyrus; SOG.L = left superior occipital gyrus; IOG.L = left inferior occipital gyrus.

between the five single-layer frequency-specific MEG networks and demonstrated that the vulnerable hub regions in patients with Alzheimer's disease lost their functional roles played across layers compared to the same regions in healthy control subjects.

Correlation between multiplex centrality metrics and MMSE/CSF biomarkers

The multiplex centrality metrics in the right precuneus (o_i, c_i, e_i) and left hippocampus (c_i), and the hub disruption index (o_i) in patients with Alzheimer's disease were significantly positively correlated with the MMSE scores (Fig. 7A–D), indicating that cognitive function is related to the vulnerability of the hub regions in patients with Alzheimer's disease. No significant correlations were found between the MMSE scores and the multiplex centrality metrics in the occipital hubs.

In patients with Alzheimer's disease, the hub disruption index of local efficiency correlated positively with the level of CSF amyloid-β_{42} (Spearman's $r = 0.4626$, $P = 0.024$) (Fig. 7F), indicating that the vulnerability of hub areas in patients with Alzheimer's disease was associated with lower

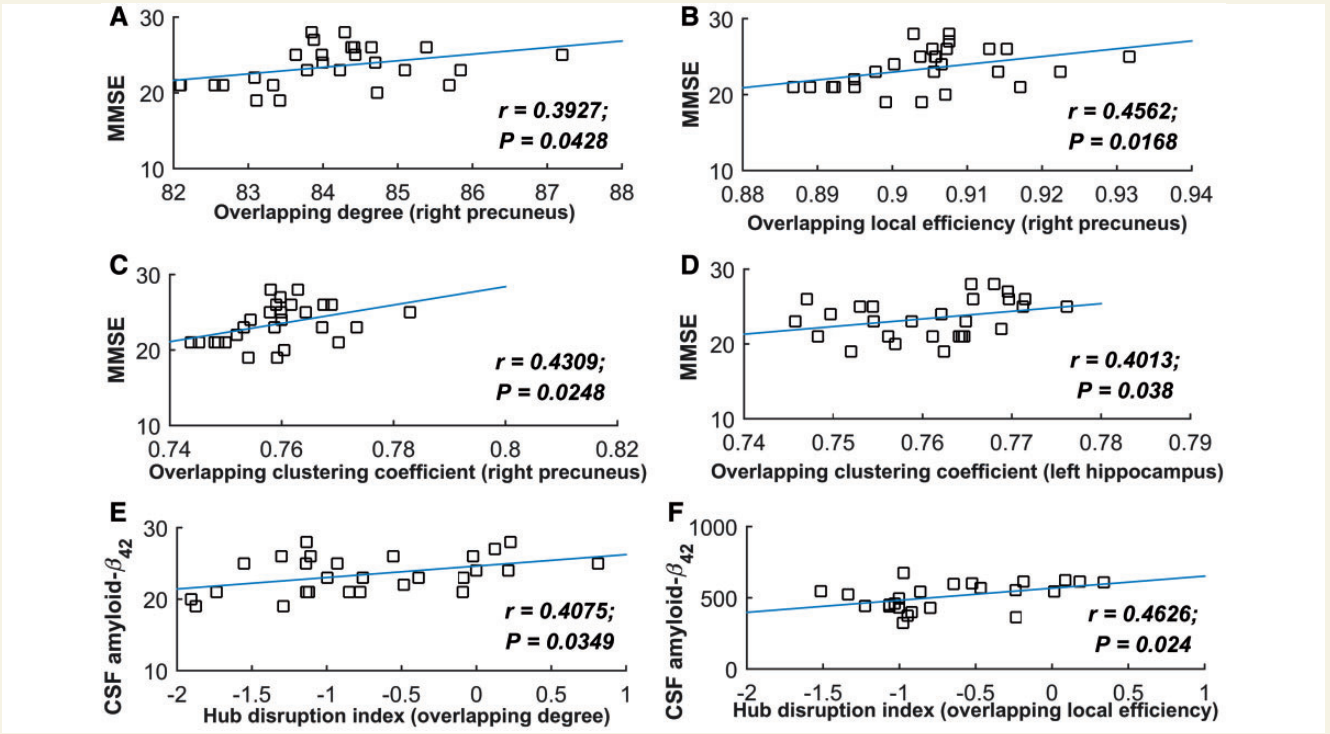

Figure 7 Perturbed cognitive function and abnormal CSF amyloid-β42 levels correlated positively with the vulnerability of the hub regions. For the patients with Alzheimer's disease only (uncorrected *P*-values): the correlations between MMSE scores and multiplex nodal centrality metrics in vulnerable regions (**A–D**), and between MMSE scores and the hub disruption index for multiplex overlapping weighted degree (**E**). The correlations between CSF amyloid-β_{42} and the hub disruption index for multiplex overlapping weighted local efficiency (**F**).

levels of CSF amyloid-β_{42}. No significant correlations were found between the hub disruption index and the levels of CSF p-tau and tau.

Discussion

We analysed MEG-based resting-state multiplex networks in patients with Alzheimer's disease and controls. No evident differences between the two groups were found when comparing the topologies of frequency-specific networks individually. In contrast, in comparison with controls, multiplex networks in patients with Alzheimer's disease were characterized by a loss of nodal centrality in hub regions such as the left hippocampus, posterior default model network and occipital regions, as well as different nodal heterogeneity of these vulnerable regions across layers. In patients with Alzheimer's disease, the damage to highly central hub areas correlated positively to more abnormal levels of CSF amyloid-β_{42} and to perturbed cognitive function measured by MMSE scores.

Our multiplex network analysis is the first MEG source-space network study reporting the selectively vulnerable hubs involving the hippocampus, posterior DMN and occipital regions in patients with Alzheimer's disease. Except for the occipital regions, the vulnerability of the hippocampus and posterior DMN in patients with Alzheimer's disease has consistently been reported in previous structural (DTI and MRI) and functional (PET and functional MRI) neuroimaging studies (Greicius *et al.*, 2004; Supekar *et al.*, 2008; Buckner *et al.*, 2009; Lo *et al.*, 2010; Crossley *et al.*, 2014). However, these specific disrupted hub regions have not been found in previous frequency-specific MEG studies (Stam *et al.*, 2009; de Haan *et al.*, 2012*a*; Canuet *et al.*, 2015). In addition, the multiplex centrality metrics were able to identify the prominent hubs located in the posterior midline (precuneus) and hippocampus in the controls, which were usually absent in frequency-specific electrophysiological studies (Brookes *et al.*, 2011*b*; Hipp *et al.*, 2011, 2012; Baker *et al.*, 2014). Therefore, integrating frequency-specific MEG functional networks into a framework of multiplex networks provides more information in support of the theoretical prediction that hub regions are particularly vulnerable in Alzheimer's disease than only considering individual frequency-specific networks.

Hubs of multiplex networks are selectively vulnerable in Alzheimer's disease

In the present study, we found that MEG-based resting-state multiplex networks in Alzheimer's disease were preferentially disrupted in hub regions, including regions in

medial temporal lobe (left hippocampus), posterior default mode network and occipital regions. The disruption of these specific hub regions in Alzheimer's disease was consistently demonstrated by different multiplex nodal centrality measures: overlapping weighted degree, overlapping weighted clustering coefficient, overlapping weighted local efficiency. Moreover, the disruption of hub areas in patients with Alzheimer's disease was further confirmed by computing the hub disruption index. Previous EEG network studies have consistently shown that posterior brain regions are disrupted in patients with Alzheimer's disease (Engels *et al.*, 2015; Yu *et al.*, 2016). Our previous sensor-space MEG network study found that the theta band nodal centrality over the left temporal lobe was disrupted (de Haan *et al.*, 2012*a*). In addition, functional MRI network studies have also identified selectively vulnerable hub regions in Alzheimer's disease, involving the DMN (Buckner *et al.*, 2009; Dai *et al.*, 2015) and hippocampus (Supekar *et al.*, 2008). Recently, a functional MRI study found that the cascading network failure in patients with Alzheimer's disease begins in the posterior DMN without evidence of amyloid plaques on PET, and then progresses to other hub regions (Jones *et al.*, 2016), which highlights the important role of posterior components of DMN in Alzheimer's disease (Stam, 2014). Performing a meta-analysis on MRI studies, Crossley and colleagues (2014) reported that in patients with Alzheimer's disease, the hubs in medial temporal and parietal regions had more MRI lesions than non-hub regions, further supporting our findings. Furthermore, our MEG study is one of the first network studies to report the disruption of specific occipital hub regions in patients with Alzheimer's disease.

Computational network models have also demonstrated that high-cost hub regions tend to be more vulnerable in Alzheimer's disease (Stam *et al.*, 2009; de Haan *et al.*, 2012*c*; Raj *et al.*, 2012). An extensive simulation study showed that abnormal network organization in patients with Alzheimer's disease, including decreased functional connectivity, selectively disrupted hub regions and more-random network topologies, could be explained by activity-dependent degeneration (de Haan *et al.*, 2012*c*). Specifically, the assumption that excessive local neuronal activity causes synaptic damage, provides a possible explanation for these network changes, including the hub vulnerability in patients with Alzheimer's disease. Our MEG-based multiplex study confirmed the hub vulnerability in patients with Alzheimer's disease. However, aforementioned modelling studies are within the framework of single-layer networks. As mentioned in the 'Introduction' section, hub nodes in multilayer networks become particularly vulnerable when random cascading failures occurs (Buldyrev *et al.*, 2010) or even when hubs are protected (Huang *et al.*, 2011). Therefore, there is a strong need for establishing multiplex network models to support our findings of hub vulnerability in multilayer networks.

The vulnerable brain regions in Alzheimer's disease played different roles across layers

The nodal centrality metrics evaluated the importance of each node for the overall efficiency of the multiplex networks. By computing the multiplex participation coefficient, we were able to quantify the participation of each node to the topology in each layer.

We reported that in patients with Alzheimer's disease, the vulnerable hub regions detected by the nodal centrality metrics had different nodal heterogeneity across layers in comparison with controls (Figs 5B and 6C). Among these vulnerable regions, the posterior DMN regions shifted from peripheral hubs in controls to connector non-hubs in patients with Alzheimer's disease, indicating that the posterior DMN regions played different functional roles across layers in the two groups. In this study, each layer corresponded to each frequency-specific MEG network. The heterogeneous connectivity patterns of posterior DMN regions across different layers in controls were disrupted in patients with Alzheimer's disease, indicating that posterior DMN regions in patients with Alzheimer's disease were not equally disrupted across layers. In contrast, other vulnerable regions such as left hippocampus, superior parietal cortex and occipital regions, showed similar nodal heterogeneity in the Alzheimer's disease and healthy control groups, indicating that these vulnerable regions were uniformly disrupted in all frequency-specific MEG networks in patients with Alzheimer's disease. Furthermore, the multiplex participation coefficients showed that the left hippocampus and superior parietal cortex were equally participating in each layer in the two groups; however, the three occipital regions had different connectivity patterns in different frequency bands in both groups. In patients with Alzheimer's disease, the different connectivity patterns of the vulnerable hub brain regions across layers indicate that hubs played different roles in different frequency bands. Therefore, it is of the essence to take all the frequency-specific networks into account simultaneously in Alzheimer's disease network analysis. Our multiplex network study provides an effective framework to integrate the frequency-specific networks.

Vulnerability of hub areas in patients with Alzheimer's disease is related to cognitive performance

Higher network efficiency of structural and functional brain networks has been shown to correlate positively with better cognitive performance (Li *et al.*, 2009; van den Heuvel *et al.*, 2009). The cognitive dysfunction in neurological diseases has been considered to be related to the disruption of the optimal balance between local segregation and global integration of neural information processing in brain networks (Bullmore and Sporns, 2009;

Stam, 2014; Petersen and Sporns, 2015). Previous brain network studies have consistently shown that Alzheimer's disease can be regarded as a cost-driven network disorder: hub regions tend to be metabolically more expensive than non-hubs (Bullmore and Sporns, 2012). Therefore, the deteriorated cognitive performance and behavioural symptoms in Alzheimer's disease could be due to the selective damage to the biologically high-cost hub regions (Buckner *et al.*, 2009; Stam *et al.*, 2009; de Haan *et al.*, 2012*c*; Crossley *et al.*, 2014).

In this study, the observed positive correlations between the multiplex nodal centrality in posterior DMN/hippocampus and the MMSE scores in patients with Alzheimer's disease indicate that the vulnerability of the hub areas has clinical relevance (Fig. 7). We reported that several components of the posterior DMN (right precuneus and inferior parietal cortices), as well as the hippocampus, were vulnerable in patients with Alzheimer's disease. This is in line with previous findings in healthy controls and patients with Alzheimer's disease. The DMN is known to play a role in many different cognitive functions (Fox and Raichle, 2007; Raichle, 2015). It has consistently been demonstrated that the DMN in early Alzheimer's disease shows an abnormal connectivity pattern, which correlates strongly with abnormal cognitive functioning (Greicius *et al.*, 2004; Buckner *et al.*, 2008, 2009; Zhou *et al.*, 2010; Menon, 2011). The precuneus plays a particularly prominent structural and functional role in healthy brains, and is involved in cognitive processes such as episodic memory and self-referential processing (Cavanna and Trimble, 2006; Fransson and Marrelec, 2008; Hagmann *et al.*, 2008; Gong *et al.*, 2009). The inferior parietal lobule, involved in attention and action processing, has also shown decreased functional connectivity and metabolism in the early course of Alzheimer's disease (Fogassi *et al.*, 2005; Singh-Curry and Husain, 2009; Wang *et al.*, 2015). Therefore, the disruption of the nodal efficiency in precuneus and inferior parietal cortex may also account for the abnormal cognitive performances in patients with Alzheimer's disease (Lehmann *et al.*, 2013). Similarly, the hippocampus acts as convergence zone in the large-scale functional connectome (Mišić *et al.*, 2014). The prominent role of hippocampus in memory processing might explain why the disruption of its hub property could lead to the early memory disturbances in patients with Alzheimer's disease (Allen *et al.*, 2007; Eichenbaum *et al.*, 2007; Battaglia *et al.*, 2011).

Relationship between hub vulnerability in Alzheimer's disease and CSF amyloid-β_{42}

CSF biomarkers (CSF amyloid-β_{42}, p-tau and tau) have been established as biomarkers for Alzheimer's disease (Blennow *et al.*, 2001). In particular, the level of CSF amyloid-β_{42} is decreased in patients with Alzheimer's disease compared with healthy controls, while levels of CSF (p) tau are increased (Mulder *et al.*, 2010; Duits *et al.*, 2014; Scheltens *et al.*, 2016). Therefore, it is reasonable to assume that there might be some relationship between the levels of CSF biomarkers and the abnormal brain network organization in Alzheimer's disease. In the present study, in patients with Alzheimer's disease the level of CSF amyloid-β_{42} was positively associated with the disruption of hub areas in the multiplex brain networks, as quantified by the hub disruption index (Fig. 7). The negative hub disruption indices in patients with Alzheimer's disease indicated that areas that were hubs in controls were disrupted in patients with Alzheimer's disease (Fig. 4), and that this related to lower levels of CSF amyloid-β_{42} (Fig. 7), providing a link with underlying pathophysiology. Our study is the first MEG network study to report the positive association between abnormal levels of CSF amyloid-β_{42} and hub disruption in the multiplex brain networks. To date, only few studies have explored the impact of CSF amyloid-β_{42} on functional connectivity in patients with Alzheimer's disease. One MEG resting-state functional connectivity study has reported that MCI patients with abnormal CSF amyloid-β_{42} show decreased functional connectivity of the medial temporal regions and posterior DMN regions in specific frequency bands (Canuet *et al.*, 2015). In a resting-state functional MRI study, decreased CSF amyloid-β_{42} was also shown to be associated with reduced functional connectivity between posterior cingulate and medial temporal regions (Wang *et al.*, 2013). Moreover, a previous PET amyloid imaging study has demonstrated that amyloid-β_{42} deposition in patients with Alzheimer's disease is preferentially located in cortical hub areas (Buckner *et al.*, 2009). The low level of CSF amyloid-β_{42} indicates the increased amyloid-β_{42} deposition in the brain. Therefore, our observations provide a possible link between hub vulnerability and amyloid pathology in CSFs and brain regions of patients with Alzheimer's disease. On the other hand, the current study cannot provide the evidence of correlations between the levels of CSF (p) tau and multiplex network measures, which could be due to the limited size of our patient sample. Future studies could use larger group of patients with Alzheimer's disease to investigate the potential correlations between the levels of CSF (p) tau and multiplex network measures.

Frequency-specific analysis or multiplex network analysis?

Neuronal activity as measured by MEG recordings shows rich temporal structure in a wide range of frequencies, which are considered to be in involved in different cognitive processes (Wang, 2010). As a consequence, MEG data have conventionally been analysed in different frequency bands (Siegel *et al.*, 2012; Stam and van Straaten, 2012; Stam, 2014).

Previous MEG studies in both patients with Alzheimer's disease and healthy control subjects have shown that the functional connectivity pattern, network topologies and the direction of information flow in large-scale functional networks are frequency-specific (Bassett *et al.*, 2006, 2009; Stam *et al.*, 2009; Brookes *et al.*, 2011*b*; Hipp *et al.*, 2012; Lopes da Silva, 2013; Hillebrand *et al.*, 2016; Yu *et al.*, 2016). Here, we integrated five frequency-band specific MEG networks in a multiplex network framework. Our MEG multiplex network study provides a powerful framework to not only detect the vulnerable hub areas, but also reflect the heterogeneous connectivity patterns of the vulnerable hubs in patients with Alzheimer's disease. Noticeably, these findings could not be revealed in a frequency-specific analysis (Fig. 3). Thus, the multiplex network measures not only enhanced the sensitivity of differentiation between patients with Alzheimer's disease and controls compared with frequency-specific analyses, but also revealed the interrelationship between functional networks in different frequency bands in Alzheimer's disease.

Nonetheless, we do not intend to doubt or ignore the frequency-specific properties of MEG networks. In fact, the nodal heterogeneity of MEG multiplex networks confirmed the underlying diverse topologies of frequency-band specific networks (Figs 5B and 6C), and demonstrated that frequency-specific networks do not act as independent entities, but interact with each other. The coordination and cooperation of frequency-specific networks are possibly a reflection of the observations that different frequencies do play different roles in cognitive and behavioural processes, but that optimal cognition also requires integration of these different processes. Disruption of the integrated framework (multiplex networks), such as in Alzheimer's disease, can therefore lead to abnormal cognitive and behavioural symptoms, which is indeed what we observed (Fig. 7).

Strengths, limitations and future direction

Our current study has a number of strong points: (i) multiplex network analysis could largely reduce the potential bias by multiple comparisons in frequency-specific network analysis; (ii) using PLI as a measure of functional connectivity reduces the bias due to field spread and/or signal leakage (Stam *et al.*, 2007*b*; Hillebrand *et al.*, 2012; Porz *et al.*, 2014), and we showed that the observed group differences of multiplex network measures were not driven by secondary leakage (Supplementary material); (iii) MEG network analysis in source-space using a standard atlas aids the multimodal comparisons between our multiplex network analysis and previous structural (e.g. DTI) and functional network analyses (e.g. functional MRI); (iv) we explored the overall nodal efficiency of the multiplex networks using different centrality metrics: the key findings were consistent for all the centrality metrics; (v) to avoid the potential biases from the differences of the magnitudes of link weights between layers, we reanalysed our data by first ranking the link weights within each layer. We found that the key findings were consistent (Supplementary Figs 1 and 2) across approaches; and (vi) by performing both group- and subject-level permutation tests for the comparisons of multiplex measures, we reduced potential biases (i.e. differences in statistical power and sensitivity to outliers) that either approach may have.

There are also several limitations that should be mentioned. Our results may have been influenced by methodological choices such as the manual selection of artefact-free epochs. However, the selected epochs were checked for quality and signs of drowsiness by an experienced independent researcher. Furthermore, the modest sample size might be a limitation. All patients with Alzheimer's disease included in this paper had pathological biomarkers suggestive for Alzheimer's disease obtained by either CSF or by amyloid PET scanning, but the amyloid status of the healthy control groups was unknown. Therefore we cannot exclude that several healthy controls actually had amyloid pathology and/or neuronal damage as well. To reduce the risk, we excluded four control subjects with abnormal results on cognitive testing. Furthermore, as our study is one of the first exploratory studies regarding the relationships between MMSE scores and multiplex network metrics, and between CSF biomarkers and the hub disruption indices, we did not correct for multiple testing in the *post hoc* correlation analyses. Instead, we reported the exact *P*-values for the reader's interpretation.

In healthy brains, the pattern of functional networks is partially determined by the underlying structural networks (Honey *et al.*, 2007, 2009; Ponten *et al.*, 2010; Mišić *et al.*, 2015; Stam *et al.*, 2016). However, the essential relationship between structural and functional networks in Alzheimer's disease is largely unknown. In this MEG study, we found that hub regions in hippocampus and posterior DMN were selectively vulnerable in patients with Alzheimer's disease, which is consistent with the findings in previous studies using other neuroimaging modalities (Crossley *et al.*, 2014). The multiplex framework allows for the integration of multimodal neuroimaging data, such as functional (MEG, PET and functional MRI) and structural networks (DTI and MRI) (Sporns, 2014). In that case, the interaction between the functional and structural networks can be studied under the unified framework of multiplex network, not only for patients with Alzheimer's disease, but also for healthy controls and for other brain disorders. Furthermore, in this study, we constructed multiplex networks by integrating five frequency-specific MEG weighted networks without considering the cross-frequency couplings between different brain regions, and applied the multiplex network measures developed by Battiston *et al.* (2014) to characterize the topological structure of the multiplex networks. However, one recent multilayer MEG connectivity study (Brookes *et al.*, 2016) constructed a super-adjacency matrix consisting of both within-frequency

and cross-frequency couplings. However, no multiplex network measures were computed in the study by Brookes *et al.* (2016). One recent multilayer functional MRI network study (De Domenico *et al.*, 2016) applied a multilayer centrality measure (De Domenico *et al.*, 2015) by extending the PageRank centrality to multilayer functional MRI networks, and found the multilayer hubs characterized by the centrality measure improved the differentiation between healthy controls and patients with schizophrenia. To date, there is no generally accepted optimal approach to characterize the topological structure of the multilayer networks consisting of cross-layer links (cross-frequency couplings in functional brain networks) between same or different nodes (Boccaletti *et al.*, 2014). In future studies, it is important to develop and apply multilayer network measures which are appropriate for functional brain studies. Moreover, Fig. 6 shows that the patients with Alzheimer's disease and healthy controls were clearly differentiated in the 2D $P_i - o_i$ plane. Therefore, combining machine learning approaches such as random forest or support vector machine with the performed multiplex network analyses could easily distinguish the two clinical groups, which is of interest for future study (Zanin *et al.*, 2016).

Conclusion

In the present study, we used a multiplex network framework to investigate the interaction between the MEG frequency-specific functional networks in patients with Alzheimer's disease and healthy control subjects. Using multiplex network metrics, functional networks in patients with Alzheimer's disease were characterized as more heterogeneous compared to those in healthy controls. We demonstrated that the hub regions, in particular in the hippocampus, posterior DMN regions and occipital areas, were preferentially affected, and that the hub vulnerability of these regions correlated positively with the cognitive deterioration and the abnormal accumulation levels of amyloid-β plaques in cerebrospinal fluid, which may augment the underlying neuropathological cascade in Alzheimer's disease.

Acknowledgements

The authors would like to thank Prejaas Tewarie for pointing out the relevance of applying the concept of multiplex network and related measures presented in the paper by Battiston *et al.* (2014) for MEG network analysis. We thank Ida Nissen for performing quality checks on the selected epochs. We also thank Peter-Jan Ris, Ndedi Sijsma, Karin Plugge, Marlous van den Hoek and Nico Akeman for data acquisition. We thank all patients and controls for their participation.

Funding

Research of the VUmc Alzheimer Center is part of the neurodegeneration research program of the Neuroscience Campus Amsterdam. The VUmc Alzheimer Center is supported by Alzheimer Nederland and Stichting VUmc funds. Meichen Yu is supported by the China Scholarship Council (CSC). Marjolein Engels is supported by Alzheimer Nederland.

Supplementary material

Supplementary material is available at *Brain* online.

References

Achard S, Delon-Martin C, Vértes PE, Renard F, Schenck M, Schneider F, et al. Hubs of brain functional networks are radically reorganized in comatose patients. Proc Natl Acad Sci USA 2012; 109: 20608–13.

Albert R, Jeong H, Barabási AL. Error and attack tolerance of complex networks. Nature 2000; 406: 378–82.

Allen G, Barnard H, McColl R, Hester AL, Fields JA, Weiner MF, et al. Reduced hippocampal functional connectivity in Alzheimer disease. Arch Neurol 2007; 64: 1482–7.

Arendt T. Synaptic degeneration in Alzheimer's disease. Acta Neuropathol 2009; 118: 167–79.

Baker AP, Brookes MJ, Rezek IA, Smith SM, Behrens T, Probert Smith PJ, et al. Fast transient networks in spontaneous human brain activity. Elife 2014; 3: e01867.

Ballard C, Gauthier S, Corbett A, Brayne C, Aarsland D, Jones E. Alzheimer's disease. Lancet 2011; 377: 1019–31.

Barkley GL. Controversies in neurophysiology. MEG is superior to EEG in localization of interictal epileptiform activity: Pro. Clin Neurophysiol 2004; 115: 1001–9.

Bassett DS, Meyer-Lindenberg A, Achard S, Duke T, Bullmore E. Adaptive reconfiguration of fractal small-world human brain functional networks. Proc Natl Acad Sci USA 2006; 103: 19518–23.

Bassett DS, Bullmore ET, Meyer-Lindenberg A, Apud JA, Weinberger DR, Coppola R. Cognitive fitness of cost-efficient brain functional networks. Proc Natl Acad Sci USA 2009; 106: 11747–52.

Battaglia FP, Benchenane K, Sirota A, Pennartz CM, Wiener SI. The hippocampus: hub of brain network communication for memory. Trends Cogn Sci 2011; 15: 310–18.

Battiston F, Nicosia V, Latora V. Structural measures for multiplex networks. Phys Rev E 2014; 89: 032804.

Baumgartner C. Controversies in neurophysiology. MEG is superior to EEG in localization of interictal epileptiform activity: Con. Clin Neurophysiol 2004; 115: 1010–20.

Benjamini Y, Hochberg Y. Controling the false discovery rate: a practical and powerful approach to multiple testing. J Roy Stat Soc B Met 1995; 57: 289–300.

Boccaletti S, Bianconi G, Criado R, del Genio CI, Gómez-Gardeñes J, Romance M, et al. The structure and dynamics of multilayer networks. Phys Rep 2014; 544: 1–122.

Blennow K, Vanmechelen E, Hampel H. CSF total tau, Abeta42 and phosphorylated tau protein as biomarkers for Alzheimer's disease. Mol Neurobiol 2001; 24: 87–97.

Brookes MJ, Hale JR, Zumer JM, Stevenson CM, Francis ST, Barnes GR, et al. Measuring functional connectivity using MEG: methodology and comparison with fcMRI. Neuroimage 2011a; 56: 1082–104.

Brookes MJ, Woolrich M, Luckhoo H, Price D, Hale JR, Stephenson MC, et al. Investigating the electrophysiological basis of resting state networks using magnetoencephalography. Proc Natl Acad Sci USA 2011b; 108: 16783–8.

Brookes MJ, Tewarie PK, Hunt BA, Robson SE, Gascoyne LE, Liddle EB, et al. A multi-layer network approach to MEG connectivity analysis. Neuroimage 2016; 132: 425–38.

Buckner RL, Snyder AZ, Shannon BJ, LaRossa G, Sachs R, Fotenos AF, et al. Molecular, structural, and functional characterization of Alzheimer's disease: evidence for a relationship between default activity, amyloid, and memory. J Neurosci 2005; 25: 7709–17.

Buckner RL, Andrews-Hanna JR, Schacter DL. The brain's default network: anatomy, function, and relevance to disease. Ann N Y Acad Sci 2008; 1124: 1–38.

Buckner RL, Sepulcre J, Talukdar T, Krienen FM, Liu H, Hedden T, et al. Cortical hubs revealed by intrinsic functional connectivity: mapping, assessment of stability, and relation to Alzheimer's disease. J Neurosci 2009; 29: 1860–73.

Buldú JM, Bajo R, Maestú F, Castellanos N, Leyva I, Gil P, et al. Reorganization of functional networks in mild cognitive impairment. PLoS One 2011; 6: e19584.

Buldyrev SV, Parshani R, Paul G, Stanley HE, Havlin S. Catastrophic cascade of failures in interdependent networks. Nature 2010; 464): 1025–8.

Bullmore ET, Sporns O. Complex brain networks: graph theoretical analysis of structural and functional systems. Nat Rev Neurosci 2009; 10: 186–98.

Bullmore ET, Sporns O. The economy of brain network organization. Nat Rev Neurosci 2012; 13: 336–49.

Canuet L, Pusil S, López ME, Bajo R, Pineda-Pardo JÁ, et al. Network disruption and cerebrospinal fluid amyloid-beta and phospho-tau levels in mild cognitive impairment. J Neurosci 2015; 35: 10325–30.

Cardillo A, Gómez-Gardeñes J, Zanin M, Romance M, Papo D, del Pozo F, et al. Emergence of network features from multiplexity. Sci Rep 2013; 3: 1344.

Cavanna AE, Trimble MR. The precuneus: a review of its functional anatomy and behavioural correlates. Brain 2006; 129 (Pt 3): 564–83.

Cheyne D, Bostan AC, Gaetz W, Pang EW. Event-related beamforming: a robust method for presurgical functional mapping using MEG. Clin Neurophysiol 2007; 118: 1691–704.

Corsi-Cabrera M, Galindo-Vilchis L, del-Río-Portilla Y, Arce C, Ramos-Loyo J. Within-subject reliability and inter-session stability of EEG power and coherent activity in women evaluated monthly over nine months. Clin Neurophysiol 2007; 118: 9–21.

Crossley NA, Mechelli A, Scott J, Carletti F, Fox PT, McGuire P, et al. The hubs of the human connectome are generally implicated in the anatomy of brain disorders. Brain 2014; 137 (Pt 8): 2382–95.

Dai Z, Yan C, Li K, Wang Z, Wang J, Cao M, et al. Identifying and mapping connectivity patterns of brain network hubs in Alzheimer's disease. Cereb Cortex 2015; 25: 3723–42.

De Domenico M, Solé-Ribalta A, Omodei E, Gómez S, Arenas A. Ranking in interconnected multilayer networks reveals versatile nodes. Nat Commun 2015; 6: 6868.

De Domenico M, Sasai S, Arenas A. Mapping multiplex hubs in human functional brain networks. Front Neurosci 2016; 10: 326.

de Haan W, Pijnenburg YA, Strijers RL, Van der Made Y, Van der Flier WM, Scheltens P, et al. Functional neural network analysis in frontotemporal dementia and Alzheimer's disease using EEG and graph theory. BMC Neurosci 2009; 10: 101.

de Haan W, van der Flier WM, Wang H, Van Mieghem PF, Scheltens P, Stam CJ. Disruption of functional brain networks in Alzheimer's disease: what can we learn from graph spectral analysis of resting-state magnetoencephalography? Brain Connect 2012a; 2: 45–55.

de Haan W, van der Flier WM, Koene T, Smits LL, Scheltens P, Stam CJ. Disrupted modular brain dynamics reflect cognitive dysfunction in Alzheimer's disease. Neuroimage 2012b; 59: 3085–3093.

de Haan W, Mott K, van Straaten ECW, Scheltens P, Stam CJ. Activity dependent degeneration explains hub vulnerability in Alzheimer's disease. PLoS Comput Biol 2012c; 8: e1002582.

Drzezga A, Becker JA, Van Dijk KR, Sreenivasan A, Talukdar T, Sullivan C, et al. Neuronal dysfunction and disconnection of cortical hubs in non-demented subjects with elevated amyloid burden. Brain 2011; 134 (Pt 6): 1635–46.

Dubois B, Hampel H, Feldman HH, Scheltens P, Aisen P, Andrieu S, et al. Preclinical Alzheimer's disease: definition, natural history, and diagnostic criteria. Alzheimers Dement 2016; 12: 292–323.

Duits FH, Teunissen CE, Bouwman FH, Visser PJ, Mattsson N, Zetterberg H, et al. The cerebrospinal fluid "Alzheimer profile": easily said, but what does it mean? Alzheimers Dement 2014; 10: 713–23.e2.

Eichenbaum H, Yonelinas AP, Ranganath C. The medial temporal lobe and recognition memory. Annu Rev Neurosci 2007; 30: 123–52.

Engel AK, Gerloff C, Hillgetag CC, Nolte G. Intrinsic coupling modes: multiscale interactions in ongoing brain activity. Nat Rev Neurosci 2013; 80: 867–86.

Engels MM, Stam CJ, van der Flier WM, Scheltens P, de Waal H, van Straaten EC. Declining functional connectivity and changing hub locations in Alzheimer's disease: an EEG study. BMC Neurol 2015; 15: 145.

Engels MM, Hillebrand A, van der Flier WM, Stam CJ, Scheltens P, van Straaten EC. Slowing of hippocampal activity correlates with cognitive decline in early onset Alzheimer's disease. An MEG study with virtual electrodes. Front Hum Neurosci 2016; 10: 238.

Fogassi L, Ferrari PF, Gesierich B, Rozzi S, Chersi F, Rizzolatti G. Parietal lobe: from action organization to intention understanding. Science 2005; 308: 662–7.

Fornito A, Zalesky A, Breakspear M. The connectomics of brain disorders. Nat Rev Neurosci 2015; 16: 159–72.

Fox MD, Raichle ME. Spontaneous fluctuations in brain activity observed with functional magnetic resonance imaging. Nat Rev Neurosci 2007; 8: 700–11.

Fransson P, Marrelec G. The precuneus / posterior cingulate cortex plays a pivotal role in the default mode network: evidence from a partial correlation network analysis. Neuroimage 2008; 42: 1178–84.

Gong G, He Y, Concha L, Lebel C, Gross DW, Evans AC, et al. Mapping anatomical connectivity patterns of human cerebral cortex using *in vivo* diffusion tensor imaging tractography. Cereb Cortex 2009; 19: 524–36.

Greicius MD, Srivastava G, Reiss AL, Menon V. Default-mode network activity distinguishes Alzheimer's disease from healthy aging: evidence from functional MRI. Proc Natl Acad Sci USA 2004; 101: 4637–42.

Greicius M. Resting-state functional connectivity in neuropsychiatric disorders. Curr Opin Neurol 2008; 21: 424–30.

Guimerà R, Nunes Amaral LA. Functional cartography of complex metabolic networks. Nature 2005; 433: 895–900.

Hagmann P, Cammoun L, Gigandet X, Meuli R, Honey CJ, Wedeen VJ, et al. Mapping the structural core of human cerebral cortex. PLoS Biol 2008; 6: e159.

Havlin S, Stanley HE, Bashan A, Gao J, Kenett DY. Percolation of interdependent network of networks. Chaos Soliton Fract 2015; 72: 4–19.

He Y, Chen Z, Evans A. Structural insights into aberrant topological patterns of large-scale cortical networks in Alzheimer's disease. J Neurosci 2008; 28: 4756–66.

Hillebrand A, Singh KD, Holliday IE, Furlong PL, Barnes GR. A new approach to neuroimaging with magnetoencephalography. Human Brain Mapping 2005; 25: 199–211.

Hillebrand A, Barnes GR, Bosboom JL, Berendse HW, Stam CJ. Frequency-dependent functional connectivity within resting-state networks: an atlas-based MEG beamformer solution. Neuroimage 2012; 59: 3909–21.

Hillebrand A, Fazio P, de Munck JC, van Dijk BW. Feasibility of clinical magnetoencephalography (MEG) functional mapping in the presence of dental artefacts. Clin Neurophysiol 2013; 124: 107–13.
Hillebrand A, Tewarie P, van Dellen E, Yu M, Carbo EW, Douw L, et al. Direction of information flow in large-scale resting-state networks is frequency dependent. Proc Natl Acad Sci USA 2016; 113: 3867–72.
Hipp JF, Engel AK, Siegel M. Oscillatory synchronization in large-scale cortical networks predicts perception. Neuron 2011; 69: 387–96.
Hipp JF, Hawellek DJ, Corbetta M, Siegel M, Engel AK. Large-scale cortical correlation structure of spontaneous oscillatory activity. Nat Neurosci 2012; 15: 884–90.
Honey CJ, Kötter R, Breakspear M, Sporns O. Network structure of cerebral cortex shapes functional connectivity on multiple time scales. Proc Natl Acad Sci USA 2007; 104: 10240–5.
Honey CJ, Sporns O, Cammoun L, Gigandet X, Thiran JP, Meuli R, et al. Predicting human resting-state functional connectivity from structural connectivity. Proc Natl Acad Sci USA 2009; 106: 2035–40.
Huang X, Gao J, Buldyrev SV, Havlin S, Stanley HE. Robustness of interdependent networks under targeted attack. Phys Rev E 2011; 83: 065101 (R).
Jensen O, Colgin LL. Cross-frequency coupling between neuronal oscillations. Trends Cogn Sci 2007; 11: 267–9.
Jensen O, Spaak E, Zumer JM. Human brain oscillations: from physiological mechanisms to analysis and cognition. In: Supek S, Aine CJ, editors. Magnetoencephalography: from signals to dynamic cortical networks. Berlin: Springer; 2014. p.359–403.
Jones DT, Knopman DS, Gunter JL, Graff-Radford J, Vemuri P, Boeve BF, et al. Cascading network failure across the Alzheimer's disease spectrum. Brain 2016; 139: 547–62.
Kivelä M, Arenas A, Barthelemy M, Gleeson JP, Moreno Y, Porter MA. Multilayer networks. J Complex Netw 2014; 2: 203–71.
Kurant M, Thiran P. Layered complex networks. Phys Rev Lett 2006; 96: 138701.
Larson-Prior LJ, Oostenveld R, Della Penna S, Michalareas G, Prior F, Babajani-Feremi A, et al. Adding dynamics to the Human Connectome Project with MEG. Neuroimage 2013; 80: 190–201.
Lehmann M, Madison CM, Ghosh PM, Seeley WW, Mormino E, Greicius MD, et al. Intrinsic connectivity networks in healthy subjects explain clinical variability in Alzheimer's disease. Proc Natl Acad Sci USA 2013; 110: 11606–11.
Li Y, Liu Y, Li J, Qin W, Li K, Yu C, et al. Brain anatomical network and intelligence. PLoS Comput Biol 2009; 5: e1000395.
Lo CY, Wang PN, Chou KH, Wang J, He Y, Lin CP. Diffusion tensor tractography reveals abnormal topological organization in structural cortical networks in Alzheimer's disease. J Neurosci 2010; 30: 16876–85.
Lopes da Silva F. EEG and MEG: relevance to neuroscience. Neuron 2013; 80: 1112–28.
Medvedovsky M, Taulu S, Bikmullina R, Ahonen A, Paetau R. Fine tuning the correlation limit of spatio-temporal signal space separation for magnetoencephalography. J Neurosci Methods 2009; 117: 203–11.
Menon V. Large-scale brain networks and psychopathology: a unifying triple network model. Trends Cogn Sci 2011; 15: 483–506.
Mišić B, Goñi J, Betzel RF, Sporns O, McIntosh AR. A network convergence zone in the hippocampus. PLOS Comput Biol 2014; 10: e1003982.
Mišić B, Betzel RF, Nematzadeh A, Goñi J, Griffa A, Hagmann P, et al. Cooperative and competitive spreading dynamics on the human connectome. Neuron 2015; 86: 1518–29.
Mulder C, Verwey NA, van der Flier WM, Bouwman FH, Kok A, van Elk EJ, et al. Amyloid-beta (1-42), total tau, and phosphorylated tau as cerebrospinal fluid biomarkers for the diagnosis of Alzheimer disease. Clin Chem 2010; 56: 248–53.
Olde Dubbelink KT, Hillebrand A, Stoffers D, Deijen JB, Twisk JW, Stam CJ, et al. Disrupted brain network topology in Parkinson's disease: a longitudinal magnetoencephalography study. Brain 2014; 137 (Pt 1): 197–207.
Palva S, Palva JM. Discovering oscillatory interaction networks with M/EEG: challenges and breakthroughs. Trends Cogn Sci 2012; 16: 219–30.
Pievani M, de Haan W, Wu T, Seeley WW, Frisoni GB. Functional network disruption in the degenerative dementias. Lancet Neurol 2011; 10: 829–43.
Petersen SE, Sporns O. Brain networks and cognitive architectures. Neuron 2015; 88: 207–19.
Ponten SC, Daffertshofer A, Hillebrand A, Stam CJ. The relationship between structural and functional connectivity: graph theoretical analysis of an EEG neural mass model. Neuroimage 2010; 52: 985–94.
Porz S, Kiel M, Lehnertz K. Can spurious indications for phase synchronization due to superimposed signals be avoided? Chaos 2014; 24: 033112.
Querfurth HW, LaFerla FM. Alzheimer's disease. N Engl J Med 2010; 362: 329–44.
Raichle ME. The brain's default mode network. Annu Rev Neurosci 2015; 38: 433–47.
Raj A, Kuceyeski A, Weiner M. A network diffusion model of disease progression in dementia. Neuron 2012; 73: 1204–15.
Rosenblum MG, Pikovsky AS, Kurths J. Phase synchronization of chaotic oscillators. Phys Rev Lett 1996; 76: 1804–7.
Robinson SE, Vrba J. Functional neuroimaging by Synthetic Aperture Magnetometry (SAM). In: Yoshimoto T, Kotani M, Kuriki S, Karibe H, Nakasato N, editors. Recent advances in biomagnetism. Sendai: Tohoku University Press; 1999. p.302–5.
Rubinov M, Sporns O. Complex network measures of brain connectivity: uses and interpretations. Neuroimage 2010; 52: 1059–69.
Scheltens P, Blennow K, Breteler MM, de Strooper B, Frisoni GB, Salloway S, et al. Alzheimer's disease. Lancet 2016; 388: 505–17.
Schoffelen JM, Gross J. Source connectivity analysis with MEG and EEG. Hum Brain Mapp 2009; 30: 1857–65.
Schöll M, Lockhart SN, Schonhaut DR, O'Neil JP, Janabi M, Ossenkoppele R, et al. PET imaging of Tau deposition in the aging human brain. Neuron 2016; 89: 971–82.
Seeley WW, Crawford RK, Zhou J, Miller BL, Greicius MD. Neurodegenerative diseases target large-scale human brain networks. Neuron 2009; 62: 42–52.
Siegel M, Donner TH, Engel AK. Spectral fingerprints of large-scale neuronal interactions. Nat Rev Neurosci 2012; 13: 121–34.
Singh-Curry V, Husain M. The functional role of the inferior parietal lobe in the dorsal and ventral stream dichotomy. Neuropsychologia 2009; 47: 1434–48.
Sperling R. Functional MRI studies of associative encoding in normal aging, mild cognitive impairment, and Alzheimer's disease. Ann N Y Acad Sci 2007; 1097: 146–55.
Sperling RA, Laviolette PS, O'Keefe K, O'Brien J, Rentz DM, Pihlajamaki M, et al. Amyloid deposition is associated with impaired default network function in older persons without dementia. Neuron 2009; 63: 178–88.
Sporns O. Contributions and challenges for network models in cognitive neuroscience. Nature Neurosci 2014; 17: 652–60.
Stam CJ, Jones BF, Manshanden I, van Cappellen van Walsum AM, Montez T, Verbunt JP, et al. Magnetoencephalographic evaluation of resting-state functional connectivity in Alzheimer's disease. Neuroimage 2006; 32: 1335–44.
Stam CJ, van Straaten ECW. The organization of physiological brain networks. Clin Neurophysiol 2012; 123: 1067–87.
Stam CJ. Modern network science of neurological disorders. Nat Rev Neurosci 2014; 15: 683–95.
Stam CJ, Jones BF, Nolte G, Breakspear M, Scheltens P. Small-world networks and functional connectivity in Alzheimer's disease. Cereb Cortex 2007a; 17: 92–9.
Stam CJ, Nolte G, Daffertshofer A. Phase lag index: assessment of functional connectivity from multi-channel EEG and MEG with

diminished bias from common sources. Hum Brain Mapp 2007b; 28: 1178–93.
Stam CJ, de Haan W, Daffertshofer A, Jones BF, Manshanden I, Van Cappellen van Walsum AM, et al. Graph theoretical analysis of magnetoencephalographic functional connectivity in Alzheimer's disease. Brain 2009; 132: 213–24.
Stam CJ. Dementia and EEG. In: Schomer DL, Lopes da Silva FH, editors. Niedermeyer's electroencephalography: basic principles, clinical applications and related fields. . Philadelphia: Lippincott Williams & Wilkins; 2011. p.375–93.
Stam CJ, Tewarie P, Van Dellen E, van Straaten EC, Hillebrand A, Van Mieghem P. The trees and the forest: characterization of complex brain networks with minimum spanning trees. Int J Psychophysiol 2014; 92: 129–38.
Stam CJ, van Straaten EC, Van Dellen E, Tewarie P, Gong G, Hillebrand A, et al. The relation between structural and functional connectivity patterns in complex brain networks. Int J Psychophysiol 2016; 103: 149–60.
Supekar K, Menon V, Rubin D, Musen M, Greicius MD. Network analysis of intrinsic functional brain connectivity in Alzheimer's disease. PLoS Comput Biol 2008; 4: e1000100.
Szell M, Lambiotte R, Thurner S. Multirelational organization of large-scale social networks in an online world. Proc Natl Acad Sci USA 2010; 107: 13636–41.
Takahashi RH, Capetillo-Zarate E, Lin MT, Milner TA, Gouras GK. Cooccurrence of Alzheimer's disease ß-amyliod and tau pathologies at synapses. Neurobiol Aging 2010; 31: 1145–52.
Taulu S, Simola J. Spatiotemporal signal space separation method for rejecting nearby interference in MEG measurements. Phys Med Biol 2006; 51: 1759–68.
Taulu S, Hari R. Removal of magnetoencephalographic artifacts with temporal signal-space separation: demonstration with single-trial auditory-evoked responses. Hum Brain Mapp 2009; 30: 1524–34.
Teunissen CE, Petzold A, Bennett JL, Berven FS, Brundin L, Comabella M, et al. A consensus protocol for the standardization of cerebrospinal fluid collection and biobanking. Neurology 2009; 73: 1914–22.
Tewarie P, Hillebrand A, Schoonheim MM, van Dijk BW, Geurts JJ, Barkhof F, et al. Functional brain network analysis using minimum spanning trees in Multiple Sclerosis: an MEG source-space study. Neuroimage 2014; 88: 308–18.
Tewarie P, Hillebrand A, van Dijk BW, Stam CJ, O'Neill GC, Van Mieghem P, et al. Integrating cross-frequency and within band functional networks in resting-state MEG: a multi-layer network approach. Neuroimage 2016; 142: 324–36.
Tijms BM, Wink AM, de Haan W, van der Flier WM, Stam CJ, Scheltens P, et al. Alzheimer's disease: connecting findings from graph theoretical studies of brain networks. Neurobiol Aging 2013; 34: 2023–36.
Tzourio-Mazoyer N, Landeau B, Papathanassiou D, Crivello F, Etard O, Delcroix N, et al. Automated anatomical labeling of activations in SPM using a macroscopic anatomical parcellation of the MNI MRI single-subject brain. Neuroimage 2002; 15: 273–89.
van Diessen E, Numan T, van Dellen E, van der Kooi AW, Boersma M, Hofman D, et al. Opportunities and methodological challenges in EEG and MEG resting state functional brain network research. Clin Neurophysiol 2015; 126: 1468–81.
van den Heuvel MP, Stam CJ, Kahn RS, Hulshoff Pol HE. Efficiency of functional brain networks and intellectual performance. J Neurosci 2009; 29: 7619–24.
van den Heuvel MP, Sporns O. Network hubs in the human brain. Trends Cogn Sci 2013; 17: 683–96.
van den Heuvel MP, Mandl RC, Stam CJ, Kahn RS, Hulshoff Pol HE. Aberrant frontal and temporal complex network structure in schizophrenia: a graph theoretical analysis. J Neurosci 2010; 30: 15915–26.
van der Flier WM, Scheltens P. Epidemiology and risk of factors of dementia. J Neurol Neurosurg Psychiatr 2005; 76: v2–7.
van der Flier WM, Pijnenburg YA, Prins N, Lemstra AW, Bouwman FH, Teunissen CE, et al. Optimizing patient care and research: the Amsterdam Dementia Cohort. J Alzheimers Dis 2014; 41: 313–27.
van Veen BD, van Drongelen W, Yuchtman M, Suzuki A. Localization of brain electrical activity via linearly constrained minimum variance spatial filtering. IEEE Trans Biomed Eng 1997; 44: 867–80.
Vecchio F, Miraglia F, Marra C, Quaranta D, Vita MG, Bramanti P, et al. Human brain networks in cognitive decline: a graph theoretical analysis of cortical connectivity from EEG data. J Alzheimers Dis 2014; 41: 113–27.
Wang L, Brier MR, Snyder AZ, Thomas JB, Fagan AM, Xiong C, et al. Cerebrospinal fluid Aβ42, phosphorylated Tau181, and resting-state functional connectivity. JAMA Neurol 2013; 70: 1242–8.
Wang XJ. Neurophysiological and computational principles of cortical rhythms in cognition. Physiol Rev 2010; 90: 1195–268.
Wang Z, Xia M, Dai Z, Liang X, Song H, He Y, et al. Differentially disrupted functional connectivity of the subregions of the inferior parietal lobule in Alzheimer's disease. Brain Struct Funct 2015; 220: 745–62.
Whalen C, Maclin EL, Fabiani M, Gratton G. Validation of a method for coregistering scalp recording locations with 3D structural MR images. Hum Brain Mapp 2008; 29: 1288–301.
Xia M, Wang J, He Y. BrainNet viewer: a network visualization tool for human brain connectomics. PLoS One 2013; 8: e68910.
Yu M, Hillebrand A, Tewarie P, Meier J, van Dijk B, Van Mieghem P, et al. Hierarchical clustering in minimum spanning trees. Chaos 2015; 25: 023107.
Yu M, Gouw AA, Hillebrand A, Tijms BM, Stam CJ, van Straaten EC, et al. Different functional connectivity and network topology in behavioral variant of frontotemporal dementia and Alzheimer's disease: an EEG study. Neurobiol Aging 2016; 42: 150–62.
Zanin M, Papo D, Sousa PA, Menasalvas E, Nicchi A, Kubik E, et al. Combining complex networks and data mining: why and how. Phys Rep 2016; 635: 1–44.
Zhou J, Greicius MD, Gennatas ED, Growdon ME, Jang JY, Rabinovici GD, et al. Divergent network connectivity changes in behavioural variant frontotemporal dementia and Alzheimer's disease. Brain 2010; 133: 1352–67.